Received May 30, 2022, accepted June 15, 2022, date of publication June 20, 2022, date of current version June 24, 2022.

*Digital Object Identifier 10.1109/ACCESS.2022.3184418*

# Adaptive Flight Control in the Presence of Limits on Magnitude and Rate

**JOSEPH E. GAUDIO[1], (Member, IEEE), ANURADHA M. ANNASWAMY[1], (Life Fellow, IEEE), MICHAEL A. BOLENDER[2], AND EUGENE LAVRETSKY[3], (Fellow, IEEE)**

[1]Department of Mechanical Engineering, Massachusetts Institute of Technology, Cambridge, MA 02139, USA
[2]Air Force Research Laboratory, Wright-Patterson AFB, OH 45433, USA
[3]The Boeing Company, Huntington Beach, CA 92647, USA

Corresponding author: Anuradha M. Annaswamy (aanna@mit.edu)

This work was supported by the Air Force Research Laboratory, Collaborative Research and Development for Innovative Aerospace Leadership (CRDInAL), Thrust 3 - Control Automation and Mechanization grant FA 8650-16-C-2642 and the Boeing Strategic University Initiative; cleared for release, case number 88ABW-2019-3550.

**ABSTRACT** Input constraints as well as parametric uncertainties must be accounted for in the design of safe control systems. This paper presents an adaptive controller for multiple-input-multiple-output (MIMO) plants with input magnitude and rate saturation in the presence of parametric uncertainties. A filter is introduced in the control path to accommodate the presence of rate limits. An output feedback adaptive controller is designed to stabilize the closed loop system even in the presence of this filter. The overall control architecture includes adaptive laws that are modified to account for the magnitude and rate limits. Analytical guarantees of stable adaptation, bounded trajectories, and satisfactory tracking are provided. Three flight control simulations with nonlinear models of the aircraft dynamics are provided to demonstrate the efficacy of the proposed adaptive controller for open loop stable and unstable systems in the presence of uncertainties in the dynamics as well as input magnitude and rate saturation.

**INDEX TERMS** Adaptive control, magnitude saturation, rate saturation, flight control.

## I. INTRODUCTION

Any advanced control system must be capable of incorporating realistic constraints on control inputs such as magnitude limits and rate limits. In flight control, such constraints are commonly present due to actuator limits. While magnitude saturation is often accounted for in the underlying control design, the nonlinearity arising from input rate saturation is often ignored. Actuator rate saturation can lead to Pilot Induced Oscillations (PIO), which expose the aircraft to the risk of failures, and in worst cases, to departing flight [1]–[3]. Crashes in the SAAB Gripen development are evidences of the latter [4], [5]. Additionally, in the event of control surface damage, additional complexities may arise if rate saturation is dominant.

Over the past four decades, adaptive control of linear time-invariant plant models in the presence of parametric uncertainties, perturbations due to bounded disturbances, and unmodeled dynamics has been studied extensively [6]–[11]. Adaptive control in the presence of magnitude constraints has been addressed in [12]–[19]. With the first set of results on this topic reported in [12], [13], references [14], [15] extended the analysis to the multiple-input state feedback case. Design of a state feedback magnitude saturation control architecture with a buffer region was shown in [16], by modifying the reference model. Reference [17] presents an application dependent architecture. A states accessible magnitude saturation adaptive control approach which leverages linear matrix inequalities is further proposed in [18], [19]. Empirical results for the indirect adaptive setting are considered in [20]. None of these references, however, provably address input rate saturation.

Rate saturation architectures have been considered in [21]–[31]. Reference [21] proposes directly differentiating the control signal in order to saturate the control rate before re-integrating the signal. References [22], [23] also propose non-adaptive, robustness based architectures. These non-adaptive architectures do not directly compensate for plant parametric uncertainty. Reference [24] proposes a state feedback indirect adaptive control architecture, while [25] proposes a direct model reference control architecture, although a matching condition is violated.

The associate editor coordinating the review of this manuscript and approving it for publication was Derek Abbott.

A state-feedback adaptive control approach which alters the reference command is further proposed in [28]. References [29], [30] proposed a rate limiter approach for the states accessible case in adaptive backstepping. The integrator anti-windup architecture presented in [26] is proposed for systems with input saturation, but does not include a proof of stability for an adaptive system and indeed may result in instability for certain adaptive systems [27]. The controller presented in this paper is significantly less restrictive than these papers in that it provides a solution for the MIMO case with guarantees of stable adaptation and bounded trajectories even for open loop unstable plants. It is assumed that the control input is subjected to a hard limit on its rate and therefore differs from our earlier work in [31] which imposed only a soft limit, i.e., the control rate was allowed to exceed the specified limits. A preliminary version of this work appeared in the thesis [32].

The problem addressed in this paper is the control and command tracking of plant dynamics in the presence of parametric uncertainties, using input-output measurements, even when the plant input is subjected to hard limits on its magnitude and rate. In order to introduce a rate limit on the control input without explicit differentiation, a filter is designed with hard saturation nonlinearities, similar to [1], [3]–[5], [21], [24], [25]. The introduction of such a filter however causes new challenges in the form of an additional lag. This in turn causes the underlying plant to have an increase in relative degree. This, and the fact that we only have outputs available for feedback, suggests the use of a MIMO adaptive controller that uses output feedback and that is applicable for a plant with higher relative degree. For this purpose, we propose an adaptive control approach that is along the lines of [33]–[37]. While the results of these papers guarantee stability, they do not consider either a magnitude or a rate-limit (and will be shown empirically to result in instability in this paper when such limits are present). The contribution of this paper is that a controller similar to [33]–[37], but augmented to account for magnitude and rate limits, can still be shown to lead to bounded solutions even in the presence of these limits. In particular, the adaptive law proposed in (40), derived from the error model in (38), as well as the proof of boundedness are novel and represent important contributions.

This paper proceeds as follows: Section II presents mathematical preliminaries. Section III describes the problem formulation of the output feedback control a plant with magnitude and rate saturation in the presence of parametric uncertainties. The adaptive control architecture is presented in Section IV. Stability analysis of the closed-loop system follows in Section V. Section VI demonstrates the efficacy of the proposed controller in a numerical simulation with a high-speed aircraft, with conclusions following in Section VII.

## II. PRELIMINARIES

The following notation is used for a MIMO plant model with $m$ inputs and $p$ outputs: $\{A, B, C\} := C(sI - A)^{-1}B$, where $s = \frac{d}{dt}$ is the differential operator. The transmission zeros of this system are defined using [34, Definition 1]. The columns of the matrix $B$ may be partitioned as $B = [b_1, b_2, \cdots, b_m]$. The input relative degree of the MIMO plant model is stated as follows.

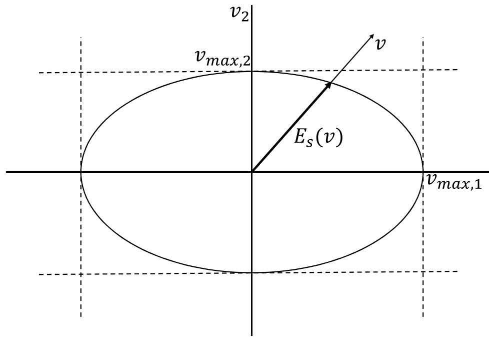


**FIGURE 1.** Elliptical saturation function for a two dimensional vector.

*Definition 1 ([35, Definition 1]):* A linear square plant given by $\{A, B, C\}$ has

a) input relative degree $r = [r_1, r_2, \ldots, r_m]^\top \in \mathbb{N}^{m\times 1}$ if
   i) $\forall j \in \{1, \ldots, m\}$, $\forall k \in \{0, \ldots, r_j - 2\}$: $CA^k b_j = 0_{p\times 1}$, and
   ii) $\text{rank}[CA^{r_1-1}b_1 \quad CA^{r_2-1}b_2 \ldots CA^{r_m-1}b_m] = m$.

b) uniform input relative degree $r \in \mathbb{N}$ if it has input relative degree $r = [r_1, r_2, \ldots, r_m]^\top$ and $r = r_1 = r_2 = \ldots = r_m$.

The following proposition describes a minimal realization where there are differentiators on the plant input.

*Proposition 1 ([35, Prop 2]):* Given a linear system $\{A, B_2, C\}$ with uniform input relative degree 2, with scalars $a_1^1 > 0$ and $a_1^0 > 0$, the following two realizations are equivalent:

1) $\dot{x}(t) = Ax(t) + B_2(a_1^1 s + a_1^0)u(t), \quad y(t) = Cx(t),$
2) $\dot{x}'(t) = Ax'(t) + B_2^1 u(t), \quad y(t) = Cx'(t),$

where

$$x'(t) = x(t) - B_2 a_1^1 u(t), \tag{1}$$

$$B_2^1 = AB_2 a_1^1 + B_2 a_1^0. \tag{2}$$

Proposition 1 may be immediately verified by using (1) and (2) in 2) to obtain 1), alongside $CB_2 = 0$ for a uniform input relative degree 2 linear system (see Definition 1. The following identity holds: $(sI - A)^{-1}s = I + (sI - A)^{-1}A$. Thus for a relative degree two input: $C(sI - A)^{-1}B_2 s = C(sI-A)^{-1}AB_2$ as $CB_2 = 0$. In this paper, elliptical saturation is considered.

*Definition 2 ([14, Page 60]):* An elliptical saturation function of a vector $v(t)$ is defined as

$$E_s(v(t), v_{\max}) = \begin{cases} v(t), & ||v(t)|| \le g(v(t)) \\ \bar{v}(t), & ||v(t)|| > g(v(t)) \end{cases} \tag{3}$$

where the function $g(v(t))$ is expressed as

$$g(v(t)) = \left( \sum_{i=1}^{m} \left[ \frac{\hat{e}_i}{(v_{\max})_i} \right]^2 \right)^{-1/2}, \tag{4}$$

where $\hat{e} = \frac{v}{||v||}$ and $\bar{v} = \hat{e}g(v)$ (see Figure 1).

Elliptical saturation ensures that the saturated input remains in the same direction (but with a smaller magnitude) as the unsaturated input. This in turn facilitates the derivation of regions of attraction for multiple input adaptive systems as in Theorem 1. It can be noted that this saturation function can be alternatively implemented using the projection operator as in [10].

## III. PROBLEM FORMULATION

We consider a class of linear plants of the form

$$\begin{aligned}\dot{x}_p(t) &= A_p x_p(t) + B_p \Lambda^*[u_p(t) + \Theta_p^{*\top} x_p(t)]\\ y_p(t) &= C_p x_p(t)\\ z(t) &= C_{pz} x_p(t) + D_{pz}\Lambda^*[u_p(t) + \Theta_p^{*\top} x_p(t)]\end{aligned} \tag{5}$$

with known matrices of dimensions: $A_p \in \mathbb{R}^{n_p\times n_p}$, $B_p \in \mathbb{R}^{n_p\times m}$, $C_p \in \mathbb{R}^{p_p\times n_p}$, $C_{pz} \in \mathbb{R}^{n_z\times n_p}$, and $D_{pz} \in \mathbb{R}^{n_z\times m}$, $n_p \geq p_p \geq m \geq n_z$. The diagonal matrix $\Lambda^* \in \mathbb{R}^{m\times m}$, and $\Theta_p^* \in \mathbb{R}^{n_p\times m}$ represent unknown constant matched uncertainty which enter the plant dynamics through the columns of $B_p$. These uncertainty locations arise in a variety of applications, including in aircraft dynamics (c.f. [10], [11], [31], [37]–[41]). Let $x_p$, $u_p$, $y_p$, and $z$ denote the plant state, plant input, plant output, and regulated output respectively. The following assumptions are made of the plant in (5):

*Assumption 1:* $\{A_p, B_p, C_p\}$ is a minimal realization;

*Assumption 2:* All transmission zeros of $\{A_p, B_p, C_p\}$ and $\{A_p, B_p, C_{pz}, D_{pz}\}$ are stable;

*Assumption 3:* $\{A_p, B_p, C_p\}$ is uniform relative degree one;

*Assumption 4:* The uncertainty $\Theta_p^*$ is bounded by a known value, i.e., $||\Theta_p^*|| < \Theta_{p,\max}$;

*Assumption 5:* The uncertainty $\Lambda^*$ is diagonal positive definite and bounded by a known value along with its inverse, i.e., $||\Lambda^*|| < \Lambda_{\max}$, $||\Lambda^{*-1}|| < \Lambda_{\text{inv},\max}$.

Assumptions 1 and 2 are standard in output feedback adaptive control [9], where the condition of stable transmission zeros of $\{A_p, B_p, C_{pz}, D_{pz}\}$ is employed to ensure controllability of an extended plant in the presence of integral tracking (to be defined) [10]. The relative degree statement in Assumption 3 is commonly satisfied for aircraft control systems. The additive uncertainty $\Theta_p^*$ is assumed to be bounded by a known value in Assumption 4. Assumption 5 states that the uncertain control effectiveness of each input path is independent of one another, upper bounded by a known value and bounded away from zero by a known value. Known bounds on the norm of the system uncertainty as in Assumptions 4 and 5 are required given that constraints will be imposed on the plant input.

The goal is to design $u_p$ so that $z$ tracks a bounded command $z_{\text{cmd}}$. To ensure a small tracking error, an integral error state $x_e$ is generated as [10]

$$\dot{x}_e(t) = z(t) - z_{\text{cmd}}(t). \tag{6}$$

### A. RATE SATURATION

The goal of this paper is to design an adaptive controller that will accommodate the parametric uncertainties in (5) and carry out the desired tracking using a control input which is rate limited, and possibly magnitude limited as well. If the time derivative of the computed control input $u$ were to be available, a filtered computed control rate $u_r$ could be generated as

$$\tau\dot{u}_r(t) + u_r(t) = \dot{u}(t), \tag{7}$$

where $u$ is the output of an adaptive controller and $\tau > 0$ is a small filter time constant.[1] Equation (7) implies that for a small enough $\tau$, $u_r(t) \approx \dot{u}(t)$. One could then recover the actual output of the controller $u$ by simply integrating $u_r$ and setting it to be equal to the plant control input $u_p$ as

$$\dot{u}_p(t) = u_r(t). \tag{8}$$

Equations (7), (8) provide us with a method for generating a control input $u_p(t)$ that is rate-limited by simply replacing $u_r$ with a saturation function of $u_r$, and generate $u_p(t)$ as

$$\tau\dot{u}_r(t) + E_s(u_r(t), u_{r,\max}) = \dot{u}(t), \tag{9}$$

$$\dot{u}_p(t) = E_s(u_r(t), u_{r,\max}), \tag{10}$$

*instead* of equations (7) and (8), where $u_{r,\max}$ is the desired rate limit on the control input. We note that $u_r$ can be realized without using explicit differentiation as

$$u_r(t) = \frac{1}{\tau}(u(t) - u_p(t)), \tag{11}$$

which can be used to generate the approximate derivative $u_r$ rather than the differential form (9).

### B. MAGNITUDE SATURATION

In addition to rate saturation, it is easy to ensure that the control input $u_p$ is magnitude limited as well. For this purpose, rather than (11), we generate $u_r$ as

$$u_r(t) = \frac{1}{\tau}(E_s(u(t), u_{\max}) - u_p(t)), \tag{12}$$

where $u_{\max}$ denotes the magnitude limit of $u$. Equations (10) and (12) lead to a realization of a control input $u_p$ into the plant that is magnitude limited and rate limited, starting from the output $u$ from the adaptive controller (see Figure 2 for a schematic).

### C. SATURATION EFFECTS AS DISTURBANCES

The saturation functions in magnitude and rate are two nonlinearities. As in [12], [25], we accommodate these nonlinearities by treating their impact as additive known disturbances. In particular, defining two known disturbance terms $\Delta u$ and $\Delta u_r$ as

$$\begin{aligned}\Delta u(t) &= E_s(u(t), u_{\max}) - u(t),\\ \Delta u_r(t) &= E_s(u_r(t), u_{r,\max}) - u_r(t),\end{aligned} \tag{13}$$

[1] It should be noted that $u_r$ in (7) can be realized without explicit differentiation of $u$, as $u_r(t) = \frac{1}{\tau}u(t) - \frac{1}{\tau}\left[\frac{1}{\tau s+1}\right]u(t)$.

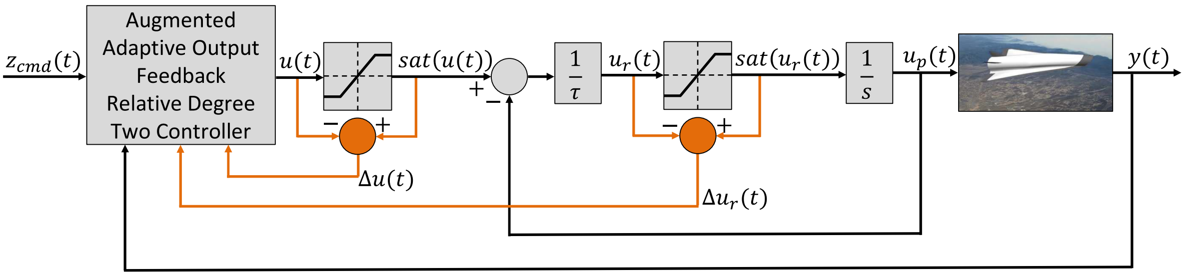


**FIGURE 2.** **Adaptive controller with input magnitude and rate limiter block diagram.**

it is easy to see that if $u$ does not reach its magnitude saturation limit $u_{\max}$, then $\Delta u(t) \equiv 0$. Similarly, if the input rate $u_r$ does not reach its rate saturation limit $u_{r,\max}$, then $\Delta u_r(t) \equiv 0$, that is, these known disturbance terms become non-zero only if the magnitude or rate limits are exceeded.

Using (12) and (13) in (10) results in a compact relation between the plant input and the control input of the form

$$\dot{u}_p(t) = -\frac{1}{\tau}u_p(t) + \frac{1}{\tau}u(t) + \frac{1}{\tau}\Delta u_2(t), \tag{14}$$

where $\Delta u_2(t) = (\Delta u(t) + \tau \Delta u_r(t))$ represents the combined effects of magnitude and rate saturation (see Figure 2 for a schematic). That is, equation (14) determines the relation between $u_p$, the plant input, and $u$, the computed control input in a compact manner.

### D. FULL PLANT EQUATIONS

We now assemble the complete plant model that includes the plant dynamics, the integral of the tracking error, and the effects of rate and magnitude saturation, which are given by equations (5), (6), and (14), respectively. This is given by

$$\begin{aligned}
\underbrace{\begin{bmatrix}\dot{x}_p(t)\\ \dot{w}_u(t)\\ \dot{x}_e(t)\end{bmatrix}}_{\dot{x}(t)} &= \underbrace{\begin{bmatrix}A_p & B_p & 0\\ 0 & -\frac{1}{\tau}I & 0\\ C_{\text{pz}} & D_{\text{pz}} & 0\end{bmatrix}}_{A}\underbrace{\begin{bmatrix}x_p(t)\\ w_u(t)\\ x_e(t)\end{bmatrix}}_{x(t)} \\
&\quad + \underbrace{\begin{bmatrix}B_p\\ 0\\ D_{\text{pz}}\end{bmatrix}}_{B_1}\Lambda^*\Theta_p^{*\top}x_p(t) + \underbrace{\begin{bmatrix}0\\ \frac{1}{\tau}I\\ 0\end{bmatrix}}_{B_2}\Lambda^*u(t) \\
&\quad + \begin{bmatrix}0\\ \frac{1}{\tau}I\\ 0\end{bmatrix}\Lambda^*\Delta u_2(t) + \underbrace{\begin{bmatrix}0\\ 0\\ -I\end{bmatrix}}_{B_z}z_{\text{cmd}}(t) \\
y(t) &= \underbrace{\begin{bmatrix}C_p & 0 & 0\\ 0 & 0 & I\end{bmatrix}}_{C}\begin{bmatrix}x_p(t)\\ w_u(t)\\ x_e(t)\end{bmatrix} \\
z(t) &= \underbrace{\begin{bmatrix}C_{\text{pz}} & D_{\text{pz}} & 0\end{bmatrix}}_{C_z}\begin{bmatrix}x_p(t)\\ w_u(t)\\ x_e(t)\end{bmatrix} + D_{\text{pz}}\Lambda^*\Theta_p^{*\top}x_p(t),
\end{aligned} \tag{15}$$

where $w_u := \Lambda^* u_p$ and the measured output is $y$. Equation (15) can be expressed in a compact form as

$$\begin{aligned}
\dot{x}(t) &= Ax(t) + B_1\Psi_1^{*\top}x(t) + B_2\Lambda^*u(t) \\
&\quad + B_2\Lambda^*\Delta u_2(t) + B_z z_{\text{cmd}}(t) \\
y(t) &= Cx(t) \\
z(t) &= C_z x(t) + D_{\text{pz}}\Psi_1^{*\top}x(t),
\end{aligned} \tag{16}$$

where $A \in \mathbb{R}^{n\times n}$, $B_1 \in \mathbb{R}^{n\times m}$, $B_2 \in \mathbb{R}^{n\times m}$, $B_z \in \mathbb{R}^{n\times n_z}$, $C \in \mathbb{R}^{p\times n}$, $C_z \in \mathbb{R}^{n_z\times n}$. The matrix of additive uncertainty is represented as $\Psi_1^{*\top} = \begin{bmatrix}\Lambda^*\Theta_p^{*\top} & 0 & 0\end{bmatrix}$ and the measured output is $y$.

Based on the structure of the full plant model in (15) it can be noted that $\{A, B_2, C\}$ is a minimal realization given Assumptions 1 and 2. In particular, Assumption 2 ensures that the inclusion of integral tracking (6) in the extended dynamics (15) preserves controllability given that $\{A_p, B_p, C_{\text{pz}}, D_{\text{pz}}\}$ does not have a transmission zero at the origin [10]. Observability of the extended dynamics (15) is preserved (and may also be enhanced) with the inclusion of integral tracking (6) as the integral tracking state $x_e$ is measured. Furthermore, it can be demonstrated that the inclusion of the filter dynamics with state $w_u$ in (15) maintains controllability and observability of the extended system, given the form of a low-pass filter in series with a controllable and observable plant with states $x_p$ and $x_e$.

Additionally, given Assumptions 2 and 3, all transmission zeros of $\{A, B_2, C\}$ are stable and $\{A, B_2, C\}$ is uniform relative degree two. It can be noticed that $B_1$ can be spanned by a linear combination of $B_2$ and $AB_2$ as $B_1 = \tau AB_2 + B_2$. Furthermore, $\Psi_1^*$ satisfies $\Psi_1^{*\top}B_2 = 0$ ($\Psi_1^*$ is not in the same input path as the computed control input) and is bounded by a known value from Assumptions 4 and 5, i.e., $||\Psi_1^*|| < \Psi_{\max} = \Theta_{p,\max}\Lambda_{\max}$.

## IV. ADAPTIVE CONTROL DESIGN

This section presents an adaptive controller for the plant model of uniform relative degree two in equation (16) whose structure is similar to that in [33]–[37]. As will be shown, modifications in the underlying adaptive laws are needed to account for the effects of input magnitude and rate saturation. Section IV-A presents the control architecture with gains designed in Section IV-B. The construction of an underlying error model that is strictly positive real is presented in Section IV-C.

### A. CONTROL ARCHITECTURE

As in any adaptive control design, we begin the control architecture discussion with the introduction of a reference model, which denotes the desired dynamics from the plant when there is no parametric uncertainty and no saturation disturbance. This corresponds to the plant model in (16) with $\Lambda^* = I$, $\Psi_1^* = 0$, and $\Delta u_2(t) = 0$. A closed-loop term is added, as in recent investigations [10], [40]–[47], which leads to a closed-loop reference model (CRM) in order to ensure smooth control inputs. Given that this problem is in output feedback, the reference model additionally serves the dual purpose as an observer [10], [42]. The use of $x_m$ to denote the state of the CRM as compared to the common observer notation of $\hat{x}$ is solely a notation choice, where both representations have appeared in the adaptive control literature. Based on the plant structure (16) in Section III, a CRM may be chosen as

$$\begin{aligned} \dot{x}_m(t) &= Ax_m(t) + B_2u_{bl}(t) + L(y(t) - y_m(t)) \\ &\quad + B_z z_{\mathrm{cmd}}(t) \\ y_m(t) &= Cx_m(t), \\ z_m(t) &= C_z x_m(t) + D_{\mathrm{pz}}u_{bl}(t), \end{aligned} \tag{17}$$

where the design of $L$ is discussed in Section IV-B. The input $u_{bl}$ is chosen so as to ensure a stable CRM, and is of the form

$$u_{bl}(t) = -Kx_m(t), \tag{18}$$

where the matrix $K \in \mathbb{R}^{n\times m}$ can be designed to provide for a desired stable reference model matrix $A_m = A - B_2K$. It can be noticed that in the presence of perfect output tracking of the reference model output ($y(t) - y_m(t) = 0$), the CRM in (17) has the form of the standard adaptive control open loop reference model with $\dot{x}_m(t) = A_m x_m(t) + B_z z_{\mathrm{cmd}}(t)$.

Given that the plant in (16) contains parametric uncertainties, an adaptive control input will be used to counter these uncertainties. The difficulty however is that the introduction of the filter in (14) causes the underlying plant dynamics to have a relative degree of two, given that the model in (5) has a relative degree of one as noted in Assumption 3. This causes the corresponding error model, derived by subtracting (17) from (16), to have a relative degree two property as well. The relative degree two property prohibits the use of a typical adaptive control input of the form of $u(t) = \Omega^\top(t)\xi(x_m(t))$, where $\Omega$ is an estimate of unknown parameters and $\xi$ is the regressor. In order to provide for a strictly positive real (SPR) error model, an extra zero must be added [9, Chapter 5]. For this purpose, we now design the computed control input $u$ as

$$u(t) = (a_1^1 s + a_1^0)\Omega^\top(t)\bar{\xi}(t), \tag{19}$$

where the variables $a_1^1 > 0$ and $a_1^0 > 0$ can be selected as desired to place the extra zero [36]. The adaptive parameter matrix $\Omega$ and regressor vector $\bar{\xi}$ are defined as

$$\Omega(t) = [\Lambda^\top(t), \Psi_1^\top(t), \Psi_2^\top(t)]^\top,$$

$$\bar{\xi}(t) = [\bar{u}_{bl}^\top(t), -x_m^\top(t), -\bar{x}_m^\top(t)]^\top, \tag{20}$$

where $\Omega$ is an estimate of $\Omega^* = [\Lambda^{*-1}, \bar{\Psi}_1^{*\top}, \bar{\Psi}_2^{*\top}]^\top$, $\bar{\Psi}_1^* = \left[\frac{\tau}{a_1^1}\Theta_p^{*\top}\ 0\ 0\right]^\top$ and $\bar{\Psi}_2^* = \left[\left(I - \tau\frac{a_1^0}{a_1^1}I\right)\Theta_p^{*\top}\ 0\ 0\right]^\top$. The following filtered signals are defined as

$$\begin{aligned} \bar{u}_{bl}(t) &= \frac{1}{a_1^1 s + a_1^0}u_{bl}(t), \\ \Delta\bar{u}_2(t) &= \frac{1}{a_1^1 s + a_1^0}\Delta u_2(t), \\ \bar{x}_m(t) &= \frac{1}{a_1^1 s + a_1^0}x_m(t). \end{aligned} \tag{21}$$

Since the elements of $\bar{\xi}$ are filtered signals, it is easy to show that (19) can be realized without explicit differentiation, provided the derivative of $\Omega$ can be directly synthesized. We will show in the following that this is indeed the case.

### B. THE DESIGN OF L

We now address the design of $L$, which is accomplished so as to ensure an underlying transfer function to be SPR. Since we begin with a non-square plant, a lemma is needed to square-up $\{A, B_2, C\}$ in order to apply the KYP lemma (c.f. [9, Lemma 2.5]). See [36] for a proof and design procedure of the contents of Lemma 1.

*Lemma 1 ([36, Lemma 5.1]):* For plant models of the form of (16) which satisfy Assumptions 1 to 3, there exists a matrix $B_{s1} \in \mathbb{R}^{n\times(p-m)}$ such that $\{A, \bar{B}_2, C\}$, where $\bar{B}_2 = [B_2, B_{s1}]$, has stable transmission zeros and nonuniform input relative degree $r_i = 2$ for $i = 1, 2, \ldots, m$ and $r_i = 1$ for $i = m+1, m+2, \ldots, p$.

The matrix $B_{s1}$ is used only in the design of $L$ as follows:

$$\bar{B}_2^1 = [B_2^1, B_{s1}], \tag{22}$$

$$S^\top = (C\bar{B}_2^1) = [S_2^\top, S_1^\top], \tag{23}$$

$$\bar{C} = SC, \tag{24}$$

$$R^{-1}(\varepsilon) = (\bar{C}\bar{B}_2^1)^{-1}\left[\bar{C}A\bar{B}_2^1 + (\bar{C}A\bar{B}_2^1)^\top\right](\bar{C}\bar{B}_2^1)^{-1} + \varepsilon I, \tag{25}$$

$$\varepsilon > \varepsilon_{\max}(A, B, \bar{C}, a_1^1, a_1^0, \Lambda_{\max}, \Psi_{\max}), \tag{26}$$

$$L = \bar{B}_2^1 R^{-1}(\varepsilon)S, \tag{27}$$

$$A_L^* = (A + B_1\Psi_1^{*\top} - LC), \tag{28}$$

where $\varepsilon > \varepsilon_{\max}$ is selected large enough to guarantee that $A_L^*$ is Hurwitz and the realization $\{A_L^*, B, SC\}$ is SPR. In summary, the closed-loop gain $L$ is chosen so as to guarantee that $\{A_L^*, B, SC\}$ is SPR. This property in turn will be used to derive the adaptive laws for adjusting $\Omega$, which is shown in the next section.

### C. SPR ERROR MODEL

This section will derive an error model and propose adaptive update laws from its SPR properties. The model tracking error is defined as $e_x(t) = x(t) - x_m(t)$. Applying (16), (19), (21), (17) and (28), the following error model may be derived:

$$\begin{aligned}\dot{e}_x(t) = A_L^* e_x(t) + B_2^1 \Lambda^* \bar{\Psi}_1^{*\top} x_m(t) \\ + B_2 \Lambda^* (a_1^1 s + a_1^0) \bar{\Psi}_2^{*\top} \bar{x}_m(t) \\ - B_2 \Lambda^* (a_1^1 s + a_1^0) \Lambda^{*-1} \bar{u}_{bl}(t) \\ + B_2 \Lambda^* (a_1^1 s + a_1^0) \Omega^\top(t) \bar{\xi}(t) \\ + B_2 \Lambda^* (a_1^1 s + a_1^0) \Delta \bar{u}_2(t). \end{aligned} \tag{29}$$

Given the undesirable differentiators in the right hand side of this equation, Proposition 1 may be applied with the modified model tracking error variable of the form

$$\begin{aligned} e_{mx}(t) = e_x(t) - B_2 \Lambda^* a_1^1 \Big[ \bar{\Psi}_2^{*\top} \bar{x}_m(t) + \Omega^\top(t) \bar{\xi}(t) \\ - \Lambda^{*-1} \bar{u}_{bl}(t) + \Delta \bar{u}_2(t) \Big]. \end{aligned} \tag{30}$$

This results in a modified model tracking error model as

$$\begin{aligned} \dot{e}_{mx}(t) &= A_L^* e_{mx}(t) + B_2^1 \Lambda^* \tilde{\Omega}^\top(t) \bar{\xi}(t) + B_2^1 \Lambda^* \Delta \bar{u}_2(t) \\ e_y(t) &= C e_{mx}(t) = C e_x(t), \end{aligned} \tag{31}$$

where $\tilde{\Omega}(t) = \Omega(t) - \Omega^*$.

It should be noted that equation (31) cannot be used directly to determine the rules for adjusting $\Omega(t)$. Unlike the approaches in [33]–[37], there are additional terms $\Delta \bar{u}_2(t)$ due to the presence of magnitude and rate saturation. It can be further noted that $\Delta \bar{u}_2(t)$ is a state-dependent disturbance. It is therefore significantly difficult to prove boundedness; existing methods in [33]–[37] or the algorithms in [12]–[17] cannot be used or simply extended. The adaptive law proposed in (40), derived from the error model in (38), as well as the proof of boundedness are therefore novel and represent important contributions.

In order to eliminate the effects of $\Delta \bar{u}_2$, an implementable auxiliary signal $e_\Delta$ is introduced as

$$\begin{aligned} \dot{e}_\Delta(t) &= A_L e_\Delta(t) + B_2^1 \Omega_\Delta^\top(t) \bar{\xi}_\Delta(t) \\ e_{y,\Delta}(t) &= C e_\Delta(t). \end{aligned} \tag{32}$$

The matrix $\Omega_\Delta$ and vector $\bar{\xi}_\Delta$ are

$$\begin{aligned} \Omega_\Delta(t) &= [\hat{\Lambda}^\top(t), \hat{\Psi}_1^\top(t), \hat{\Psi}_2^\top(t)]^\top, \\ \bar{\xi}_\Delta(t) &= [\Delta \bar{u}_2^\top(t), e_\Delta^\top(t), \bar{e}_\Delta^\top(t)]^\top, \end{aligned} \tag{33}$$

where $\Omega_\Delta$ is an estimate of $\Omega_\Delta^* = [\Lambda^*, \Lambda^* \bar{\Psi}_1^{*\top}, \Lambda^* \bar{\Psi}_2^{*\top}]^\top$, and where the following filtered signal is defined:

$$\bar{e}_\Delta(t) = \frac{1}{a_1^1 s + a_1^0} e_\Delta(t). \tag{34}$$

The following is an equivalent representation of (32), which is obtained using (28) and (34):

$$\begin{aligned} \dot{e}_\Delta(t) = A_L^* e_\Delta(t) - B_2^1 \Lambda^* \bar{\Psi}_1^{*\top} e_\Delta(t) \\ - B_2 (a_1^1 s + a_1^0) \Lambda^* \bar{\Psi}_2^{*\top} \bar{e}_\Delta(t) + B_2^1 \Omega_\Delta^\top(t) \bar{\xi}_\Delta(t). \end{aligned} \tag{35}$$

To eliminate the differentiator on the right hand side of this equation, Proposition 1 can be once again applied with a modified auxiliary signal of the form

$$e_{m\Delta}(t) = e_\Delta(t) + B_2 a_1^1 [\Lambda^* \bar{\Psi}_2^{*\top} \bar{e}_\Delta(t)]. \tag{36}$$

This results in modified dynamics of the form

$$\begin{aligned} \dot{e}_{m\Delta}(t) &= A_L^* e_{m\Delta}(t) + B_2^1 \tilde{\Omega}_\Delta^\top(t) \bar{\xi}_\Delta(t) + B_2^1 \Lambda^* \Delta \bar{u}_2(t) \\ e_{y,\Delta}(t) &= C e_{m\Delta}(t) = C e_\Delta(t), \end{aligned} \tag{37}$$

where $\tilde{\Omega}_\Delta(t) = \Omega_\Delta(t) - \Omega_\Delta^*$. To remove the effects of $\Delta \bar{u}_2$ the following modified augmented error ($e_{mu}(t) = e_{mx}(t) - e_{m\Delta}(t)$) model is introduced:

$$\begin{aligned} \dot{e}_{mu}(t) &= A_L^* e_{mu}(t) + B_2^1 \Lambda^* \tilde{\Omega}^\top(t) \bar{\xi}(t) - B_2^1 \tilde{\Omega}_\Delta^\top(t) \bar{\xi}_\Delta(t) \\ e_{y,u}(t) &= e_y(t) - e_{y,\Delta}(t) = C e_{mu}(t). \end{aligned} \tag{38}$$

We note that $e_{y,u}(t)$ is available at each $t$ since $e_y(t)$ is measurable and $e_{y,\Delta}(t)$ is a known signal that can be computed at each time $t$.

*Lemma 2 ([36, Lemma 5.3]):* Given $L \in \mathbb{R}^{n \times p}$ in (27) and $S \in \mathbb{R}^{p \times p}$ in (23), $\varepsilon$ in (26), and with Assumptions 1 to 5, for plant models of the form of (16), the transfer function $\{A_L^*, \bar{B}_2^1, SC\}$ is strictly positive real.

Lemma 2 also implies that $\{A_L^*, B_2^1, S_2 C\}$ is SPR given the partitions in (22) and (23). Thus given the structure of the modified augmented error model in (38), the adaptive parameters $\Omega$ and $\Omega_\Delta$ can be updated as

$$\dot{\Omega}(t) = -\Gamma_\Omega \bar{\xi}(t) e_{y,u}^\top(t) S_2^\top, \tag{39}$$

$$\dot{\Omega}_\Delta(t) = \Gamma_{\Omega_\Delta} \bar{\xi}_\Delta(t) e_{y,u}^\top(t) S_2^\top, \tag{40}$$

where $\Gamma_\Omega > 0$ and $\Gamma_{\Omega_\Delta} > 0$ are adaptive update gains.

A few comments regarding the two update laws are in order. Equation (39) represents a standard update to address parametric uncertainties in $\Omega^*$. Equation (40) represents an update due to the effects of saturation, since once the update law and $e_\Delta(0)$ are initialized at zero, they will only change when a saturation limit is reached. The adaptive update laws in (39) and (40) along with the fact that the realization $\{(A^* - LC, B_2^1, S_2 C)\}$ is SPR provides the foundation for stable adaptation. This is established in the next section.

## V. STABILITY ANALYSIS

Before proceeding to state the main result of bounded trajectories, a discussion of stable adaptation is presented in Section V-A. Bounded trajectories of all remaining states is addressed in Section V-B. It can be noted that due to the presence of saturation, not all signals can be tracked and thus results are local in nature. Local stability results will be shown to be proportional to the level of saturation and uncertainty.

### A. STABLE ADAPTATION

We consider a candidate Lyapunov function of the form

$$\begin{aligned} V(e_{mu}(t), \tilde{\Omega}(t), \tilde{\Omega}_\Delta(t)) = e_{mu}^\top(t) P e_{mu}(t) \\ + Tr\left[\tilde{\Omega}^\top(t) \Gamma_\Omega^{-1} \tilde{\Omega}(t) |\Lambda^*|\right] \\ + Tr\left[\tilde{\Omega}_\Delta^\top(t) \Gamma_{\Omega_\Delta}^{-1} \tilde{\Omega}_\Delta(t)\right], \end{aligned} \tag{41}$$

where $P = P^\top > 0$ is a positive definite matrix which can be used to guarantee the SPR properties of

$\{(A_L^*, \bar{B}_2^1, SC)\}$ and satisfy

$$A_L^{*\top} P + PA_L^* = -Q < 0,$$
$$P\bar{B}_2^1 = C^\top S^\top, \tag{42}$$

for a positive definite matrix $Q = Q^\top > 0$. The following partition may be used:

$$P[B_2^1, B_{s1}] = C^\top [S_2^\top, S_1^\top]. \tag{43}$$

Taking a derivative of (41) with respect to time and using (38):

$$\dot{V}(e_{mu}(t), \tilde{\Omega}(t), \tilde{\Omega}_\Delta(t)) = e_{mu}^\top(t)(A_L^{*\top} P + PA_L^*)e_{mu}(t) + 2e_{mu}^\top(t)PB_2^1\Lambda^*\tilde{\Omega}^\top(t)\bar{\xi}(t) - 2e_{mu}^\top(t)PB_2^1\tilde{\Omega}_\Delta^\top(t)\bar{\xi}_\Delta(t) + 2Tr\left[\tilde{\Omega}^\top(t)\Gamma_\Omega^{-1}\dot{\Omega}(t)|\Lambda^*|\right] + 2Tr\left[\tilde{\Omega}_\Delta^\top(t)\Gamma_{\Omega_\Delta}^{-1}\dot{\Omega}_\Delta(t)\right]. \tag{44}$$

Applying (39), (40), and using the cyclic property of trace:

$$\dot{V}(e_{mu}(t), \tilde{\Omega}(t), \tilde{\Omega}_\Delta(t)) = e_{mu}^\top(t)(A_L^{*\top} P + PA_L^*)e_{mu}(t) + 2e_{mu}^\top(t)PB_2^1\Lambda^*\tilde{\Omega}^\top(t)\bar{\xi}(t) - 2e_{mu}^\top(t)PB_2^1\tilde{\Omega}_\Delta^\top(t)\bar{\xi}_\Delta(t) - 2e_{y,u}^\top(t)S_2^\top\Lambda^*\tilde{\Omega}^\top(t)\bar{\xi}(t) + 2e_{y,u}^\top(t)S_2^\top\tilde{\Omega}_\Delta^\top(t)\bar{\xi}_\Delta(t). \tag{45}$$

Applying $e_{y,u}(t) = Ce_{mu}(t)$ from (38), with (42) and (43):

$$\dot{V}(e_{mu}(t), \tilde{\Omega}(t), \tilde{\Omega}_\Delta(t)) = -e_{mu}^\top(t)Qe_{mu}(t) \leq 0. \tag{46}$$

Thus all of $(e_{mu}, \tilde{\Omega}, \tilde{\Omega}_\Delta)$ are bounded. This does not show that the model tracking error $e_x$ is bounded, however the following relation for the tracking error can be obtained: $||e_x(t)|| = \mathcal{O}[\sup_{\zeta\leq t} ||\Delta u_2(\zeta)||]$. Such a relation is similar to that derived in [12]–[16], where the constants in the big $\mathcal{O}$ notation are system parameters.

## B. BOUNDED TRAJECTORIES

For clarity of presentation, the constant matrices, constant scalars and time-varying scalars found in this section are defined in Appendix A. The following closed-loop system representation can be obtained through combining (12), (13), (17), (18), (19), (20), (21), and (31):

$$\dot{\chi}(t) = A_{cl}\chi(t) - B_\Omega\tilde{\Omega}^\top(t)C_{\bar{\xi}}\chi(t) + C_{\Delta\bar{u}_2}\frac{1}{a_1^1}\Delta u_2(t) + B_Z z_{\text{cmd}}(t), \tag{47}$$

where the full state of the system to be shown bounded is

$$\chi(t) = \left[\bar{x}_m^\top(t)\ x_m^\top(t)\ e_{mx}^\top(t)\ \Delta\bar{u}_2^\top(t)\right]^\top. \tag{48}$$

It can be noted from the block upper triangular structure of $A_{cl}$ in Appendix A, that its eigenvalues can be placed arbitrarily stable. This is due to the controllability properties of the underlying dynamics and the use of a closed-loop reference model (17). Showing boundedness of the state $\chi$ will result in boundedness of all of the signals in the closed-loop system given that $e_{mu}$, $\tilde{\Omega}$, and $\tilde{\Omega}_\Delta$ were shown to be bounded in Section V-A. The main challenges that arise here are due to the various combinations of scenarios of magnitude and rate saturation that can occur, which causes $\Delta\bar{u}_2$ to be non-zero. This in turn necessitates the use of multiple sub-cases that are discussed in the proof of Theorem 1 in Appendix B. Before proceeding to a discussion of the main theorem of bounded trajectories, given that the system is input constrained, the following reference command bound is required.

*Assumption 6:* The reference command $z_{\text{cmd}}$ is bounded as $||z_{\text{cmd}}(t)|| \leq z_{\text{cmd,max}}$ and is chosen such that $\rho\chi_{\min} < \chi_{\max}$, $\kappa_3 > 0$, $\kappa_8 > 0$, $\kappa_5^2 > 4\kappa_4\kappa_6$, $\kappa_5^2 > 4\kappa_9\kappa_{10}$.

Assumption 6 implies that the magnitude of the reference command is upper bounded with respect to the level of saturation and system uncertainty. The larger the level of saturation and smaller the system uncertainty, the larger the allowable command. The bound $\rho\chi_{\min} < \chi_{\max}$ can always be achieved for a provably bounded command, as for example if $z_{\text{cmd,max}} = 0$: $\chi_{\min} = 0$ and $\chi_{\max}$ is finite, with $\kappa_3 > 0$, $\kappa_8 > 0$ and $\kappa_5^2 > 4\kappa_4\kappa_6$, $\kappa_5^2 > 4\kappa_9\kappa_{10}$. Thus $\chi_{\min}$ can be seen to represent a shift in the equilibrium of the system due to tracking of $z_{\text{cmd}}$. We now state the main theorem of bounded trajectories.

*Theorem 1:* Under Assumption 6 for the system in (16) and (17), control input (19), known control disturbances (13), adaptive laws in (39), (40), and Lyapunov function (41), the closed-loop system has bounded trajectories for all $t \geq 0$ if the following two conditions are satisfied:

i) $|\chi(0)| < \frac{1}{\rho}\chi_{\max}$

ii) $\sqrt{V(0)} < \sqrt{\frac{\lambda_{\min}}{\gamma_{\max}}}\bar{\Omega}_{\max}$

Furthermore, $||\chi(t)|| < \chi_{\max}$, $\forall t > 0$ and $||e_x(t)|| = \mathcal{O}[\sup_{\zeta\leq t} ||\Delta u_2(\zeta)||]$.

*Proof:* Given that the dynamics matrix $A_{cl}$ can be chosen by design to be strictly stable as in Appendix A, it satisfies

$$A_{cl}^\top P_{cl} + P_{cl}A_{cl} < -Q_{cl},$$

where the matrix $P_{cl}$ may be computed using a positive definite matrix $Q_{cl}$. Define the following candidate Lyapunov function of the closed-loop dynamics:

$$W(\chi(t)) = \chi^\top(t)P_{cl}\chi(t). \tag{49}$$

Define the following level set, $\mathcal{B}$, of $W$:

$$\mathcal{B} : \left\{\chi(t)|W(\chi(t)) = p_{\min}\chi_{\max}^2\right\}. \tag{50}$$

The following annulus region is defined:

$$\mathcal{A} : \{\chi(t)|\chi_{\min} \leq ||\chi(t)|| \leq \chi_{\max}\}. \tag{51}$$

The proof of boundedness of the full system state follows from two steps. The first step will show that $\mathcal{B} \subset \mathcal{A}$ using condition *(ii)* of Theorem 1. Step 2 will show that $\dot{W}(\chi(t)) < 0, \forall\chi \in \mathcal{A}$. Condition *(i)* in Theorem 1 implies the following:

$$W(\chi(0)) < W(\mathcal{B}). \tag{52}$$

The two steps thus result in the following:

$$W(\chi(t)) \leq W(\chi(0)) \quad \forall t \geq 0. \tag{53}$$

Theorem 1 follows from these two steps.

*Proof Step 1:* This step shows that $\mathcal{B} \subset \mathcal{A}$. Using condition *(ii)* from Theorem 1, it can be seen that $\tilde{\Omega}_{\max} < \bar{\Omega}_{\max}$. Additionally by Assumption 6:

$$\rho \chi_{\min} < \chi_{\max}.$$

Equation (49) can be used to show that $W(\chi(t))$ is bounded from below by $p_{\min}||\chi(t)||^2 \leq W(\chi(t))$. This implies

$$||\chi(t)|| \leq \chi_{\max} \quad \forall \chi \in \mathcal{B}.$$

In a similar manner from equation (49), $W(\chi(t))$ can be bounded from above by $W(\chi(t)) \leq p_{\max}||\chi(t)||^2$. These relations imply

$$\chi_{\min} < \frac{1}{\rho}\chi_{\max} \leq ||\chi(t)||, \quad \forall \chi \in \mathcal{B}.$$

The definition of the annulus region $\mathcal{A}$ can then be used to conclude that $\mathcal{B} \subset \mathcal{A}$.

*Proof Step 2:* It can then be shown that $\dot{W}(\chi(t)) < 0$, $\forall \chi \in \mathcal{A}$. Three cases are considered. Case A considers the system not in magnitude nor rate saturation ($\Delta u = 0$, $\Delta u_r = 0$). Case B considers the system in magnitude saturation ($\Delta u \neq 0$, $\Delta u_r = 0$) and Case C considers the system in rate saturation ($\Delta u = 0$, $\Delta u_r \neq 0$). The proof of this step is located in Appendix B.

Boundedness of the state $\chi$ in equation (48) as well as boundedness of $e_{mu}$, $\tilde{\Omega}$, and $\tilde{\Omega}_\Delta$ in Section V-A is sufficient to show that all of the signals in the closed-loop system remain bounded, thus concluding the proof of Theorem 1. □

*Remark 1:* Globally bounded trajectories cannot be achieved in the presence of magnitude and rate saturation for general (possibly open loop unstable) plant models [48]. There always exists initial conditions that will cause the system to have unbounded trajectories regardless of the design of the controller. The results are thus dependent on regions of attraction, saturation levels, and the amount of uncertainty, such as those presented in Theorem 1.

*Remark 2:* If the plant dynamics are open-loop stable, equation (5) is bounded-input, bounded-output (BIBO) stable and equations (12) and (10) results in a bounded control input. Thus the state trajectory $x_p$ is bounded regardless of initial condition.

*Remark 3:* The bounds in Theorem 1 (i) and (ii) scale with system parameters listed in Appendix A. In particular, the state upper bound $\chi_{\max}$ in Theorem 1 (i) tends to infinity as the magnitude limits and rate limits tend to infinity and the uncertainty $\Omega^*$ tends to zero. The left hand side of condition (ii) of Theorem 1 decreases (is further satisfied) as the uncertainty $\Omega^*$ tends to zero.

*Remark 4:* This architecture incorporates the effects of saturation in the auxiliary signal in (32). This auxiliary signal changes in the presence of saturation and thus alters the control input through the adaptive update laws. The effect of saturation may also be incorporated in the reference model as done in the $\mu$-mod architecture [16]. A similar error model can be formulated for the $\mu$-mod architecture, thus the MIMO output feedback magnitude and rate saturation architecture presented this paper can be extended to the $\mu$-mod architecture.

## VI. FLIGHT CONTROL NUMERICAL SIMULATIONS

This section presents numerical simulation results for an open loop stable nonlinear F-16 vehicle model for both single-input-single-output (SISO) longitudinal dynamics and multiple-input-multiple-output (MIMO) lateral-directional dynamics, as well a numerical simulation of a nonlinear high-speed vehicle model for open loop unstable longitudinal dynamics. For the F-16 vehicle, the proposed adaptive controller maintains stability in the presence of input saturation and demonstrates increased performance compared to a non-adaptive controller. The benefit of the proposed adaptive controller is even more apparent for the open loop unstable high-speed vehicle dynamics, where the proposed adaptive controller provides for command tracking, whereas non-adaptive and standard adaptive responses are unacceptable.

In each numerical simulation, (a) nonlinear models are used, (b) only output measurements are assumed to be available, and (c) hard limits are imposed on the input-magnitude and the input-rate. This practically important numerical study of flight control systems with attributes (a)-(c) is the central and unique feature of this section. In each of the multiple numerical simulations presented below, we demonstrate the need for (i) an adaptive control contribution to counter uncertainties, (ii) the need to explicitly account for input limits in the adaptive control design, and (iii) the performance improvements of the proposed control architecture. Throughout this section, high fidelity nonlinear vehicle models are employed to demonstrate the efficacy of the proposed control architecture in the realistic setting of fully nonlinear aircraft dynamics.

### A. F-16 NUMERICAL SIMULATION

This section applies the adaptive controller with limiter presented in this paper to two nonlinear F-16 simulations adapted from [49]–[51]. The aircraft simulations feature nonlinear equations of motion with aerodynamic forces and moments calculated using aerodynamic parameters scheduled from aerodynamic look-up tables based on the flight condition. In the interest of space and to focus on the numerical results, the reader is referred to [49]–[51] for a description of the full nonlinear equations of motion and an in-depth discussion of the flight condition-dependent aerodynamic parameters.

A trim point for this nonlinear F-16 vehicle model was obtained at a straight and level flying condition at a velocity of 500 ft/s with an altitude of 15, 000 ft. The vehicle model was linearized about this trim point in order to obtain linearized dynamics for control design as in (5). The actuator time constants and saturation levels from the simulation documentation [50] were employed in this simulation, thus providing for physically consistent input constraints. The thrust input to the aircraft was held constant (at the trim value). As is common in the aerospace industry for

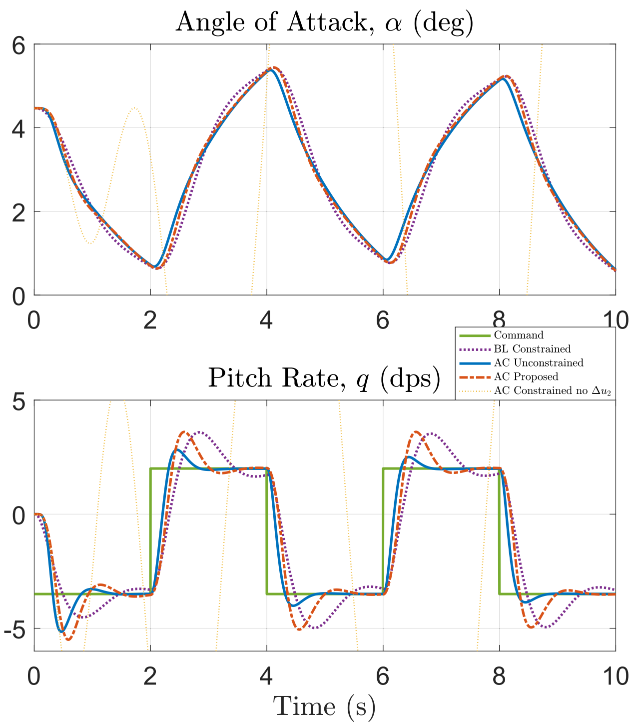


**FIGURE 3.** F-16 aircraft. Longitudinal state response comparison between baseline only control (BL Constrained), unconstrained adaptive control (AC Unconstrained), and constrained adaptive control with (AC Proposed) and without (AC Constrained no $\Delta u_2$) update law saturation modification.

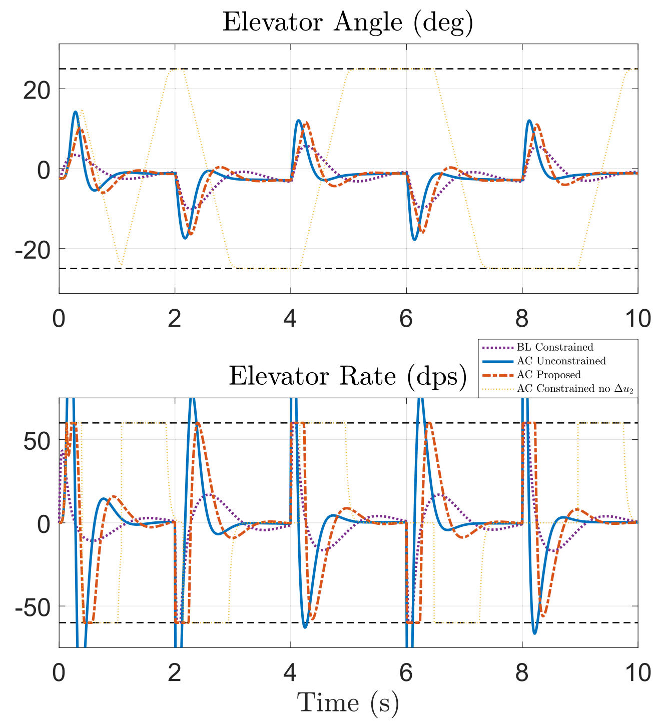


**FIGURE 4.** F-16 aircraft. Longitudinal control magnitude and rate response comparison between baseline only control (BL Constrained), unconstrained adaptive control (AC Unconstrained), and constrained adaptive control with (AC Proposed) and without (AC Constrained no $\Delta u_2$) update law saturation modification.

the purposes of control design, separate controllers were designed for the aircraft longitudinal and lateral-directional dynamics [10]. It is emphasized that the separation into longitudinal and lateral-directional dynamics is only for control design; the complete F-16 vehicle model is simulated with nonlinear equations of motion together with all coupling effects retained and flight condition-dependent aerodynamics from [49]–[51] for evaluation of the proposed controller. We note that there are significant unmeasured effects due to the nonlinear dynamics and changing aerodynamics in these simulations. As mentioned before, outputs that are measurable in practice are used in the controller, thus providing for a fully realistic flight control setting.

The longitudinal dynamics of an aircraft describe the short timescale motion in the pitch plane. The longitudinal variables for control design are given by

$$x_p = \left[\alpha \ q\right]^\top \quad u_p = \delta_e \quad y_p = q \quad z_p = q,$$

where the longitudinal state is composed of the vehicle's angle of attack $\alpha$ and pitch rate $q$. Pitch rate is both the measured and regulated variable. An elevator deflection $\delta_e$ represents the input to the dynamics. The elevator gain parameter $\tau$ and saturation levels are as follows:

$$\tau = 0.0495 \quad u_{\max} = \pm 25 \text{ deg} \quad u_{r,\max} = \pm 60 \text{ dps}.$$

The lateral-directional dynamics govern motion in the roll and yaw axes and were simulated to demonstrate the MIMO

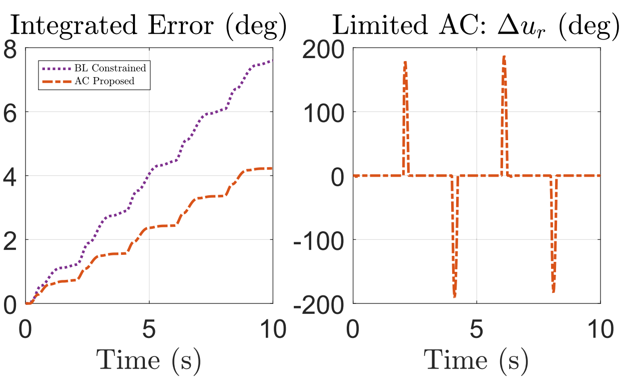


**FIGURE 5.** F-16 aircraft. Left: Integral of the absolute value of the error between the ideal (unconstrained) adaptive control pitch rate response and the constrained baseline/proposed adaptive responses of Figure 3. Right: Time history of rate saturation elevator disturbance (13) for the proposed constrained adaptive controller with saturation modification.

case. The lateral-directional subsystem is given by

$$x_p = \left[\beta \ p \ r\right]^\top \quad u_p = \left[\delta_a \ \delta_r\right]^\top \quad y_p = \left[p \ r\right]^\top \quad z_p = p,$$

where the lateral-directional state is composed of the vehicle's angle of sideslip $\beta$, roll rate $p$, and yaw rate $r$. Roll rate and yaw rate are both measured while roll rate is the regulated variable. Aileron $\delta_a$ and rudder $\delta_r$ deflections represents the inputs to the dynamics. The aileron gain parameter $\tau$ and saturation levels are as follows:

$$\tau = 0.0495 \quad u_{\max} = \pm 21.5 \text{ deg} \quad u_{r,\max} = \pm 80 \text{ dps}.$$

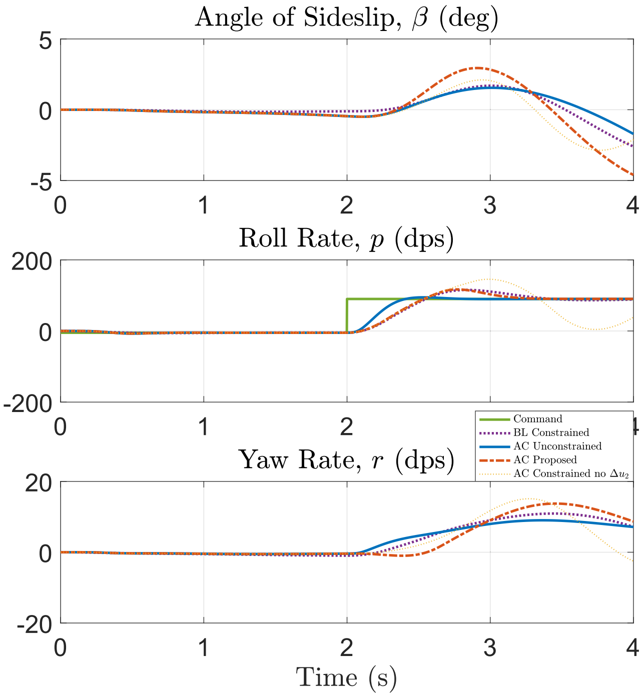


**FIGURE 6.** **F-16 aircraft. Lateral-Directional state response comparison between baseline only control (BL Constrained), unconstrained adaptive control (AC Unconstrained), and constrained adaptive control with (AC Proposed) and without (AC Constrained no $\Delta u_2$) update law saturation modification.**

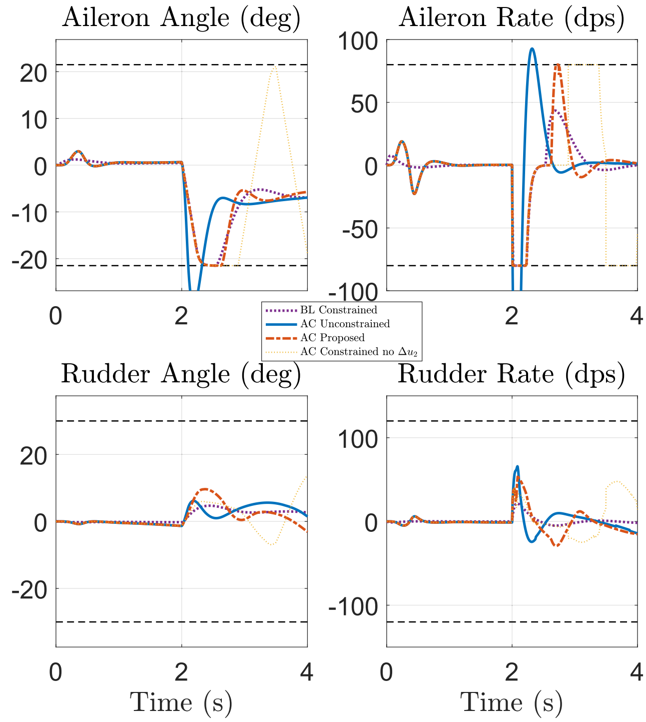


**FIGURE 7.** **F-16 aircraft. Lateral-Directional control magnitude and rate response comparison between baseline only control (BL Constrained), unconstrained adaptive control (AC Unconstrained), and constrained adaptive control with (AC Proposed) and without (AC Constrained no $\Delta u_2$) update law saturation modification.**

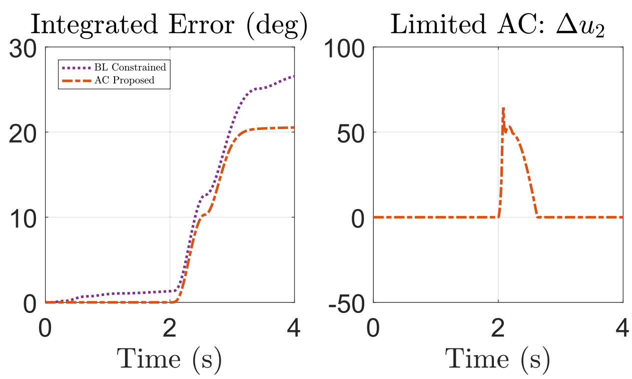


**FIGURE 8.** **F-16 aircraft. Left: Integral of the absolute value of the error between the ideal (unconstrained) adaptive control pitch rate response and the constrained baseline/proposed adaptive responses of Figure 6. Right: Time history of combined magnitude and rate saturation aileron disturbance (13) for the proposed constrained adaptive controller with saturation modification.**

The rudder gain parameter $\tau$ and saturation levels are as follows:

$$\tau = 0.0495 \quad u_{\max} = \pm 30\,\text{deg} \quad u_{r,\max} = \pm 120\,\text{dps}.$$

Separate controllers were designed for each of the two subsystems, longitudinal and lateral-directional. Integral command tracking (6) was included for both subsystems in addition to the explicit inclusion of the dynamics of each magnitude and rate saturated actuator as in (14), resulting in complete plant models as in (15), (16). The plant models for each subsystem satisfy Assumptions 1-3, as required for the adaptive control design in this paper, and further accommodate the presence of parametric uncertainties as in Assumptions 4-5.

Figures 3 and 4 show the longitudinal dynamics of the F-16 aircraft in the presence of a 75% decrease in the total pitching moment coefficient $C_m$. In this simulation, the pitch rate command is stepped every two seconds. The significant amount of uncertainty in $C_m$, results in large degradation of performance for the non-adaptive baseline-only controller (18), where it can be seen in Figure 3 that the baseline controller does not settle before the step command changes. This is prohibitive in the design of guidance controllers for aircraft which rely on step responses close to the desired response. This motivates the use of an adaptive control input in order to recover the desired performance, even in the presence of uncertainty.

To this end, the adaptive control input presented in this paper was designed as in (19). In order to counter the uncertainty and recover the desired performance, the adaptive controller (AC), if unconstrained, is seen to require large control rates, which surpass 200 dps and violate the physical actuator limits as seen in Figure 4. If the input limits are enforced for the adaptive control input as in [33]–[37], which does not include the modified error model (38) and adaptive update law (40), the closed loop system can be seen to be unstable. Figure 3 shows a stable response for the proposed adaptive controller (AC proposed) using the

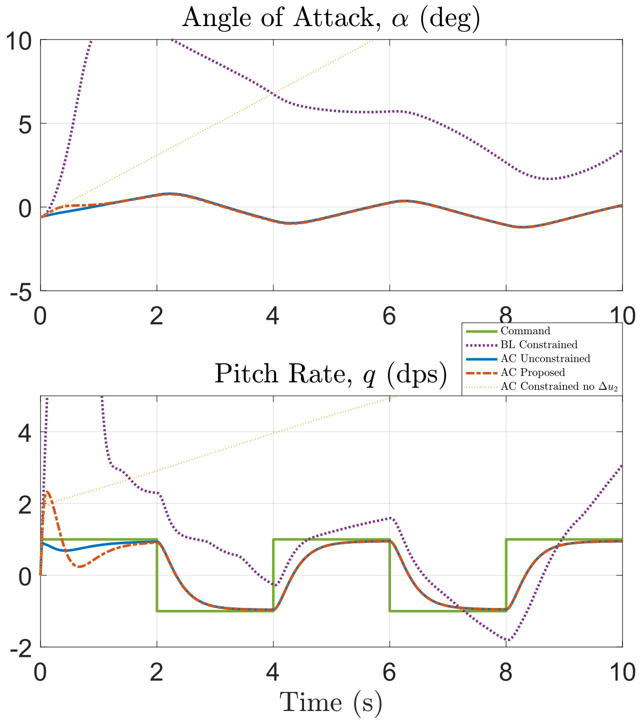


**FIGURE 9.** **High-speed Vehicle. Longitudinal state response comparison between baseline only control (BL Constrained), unconstrained adaptive control (AC Unconstrained), and constrained adaptive control with (AC Proposed) and without (AC Constrained no $\Delta u_2$) update law saturation modification.**

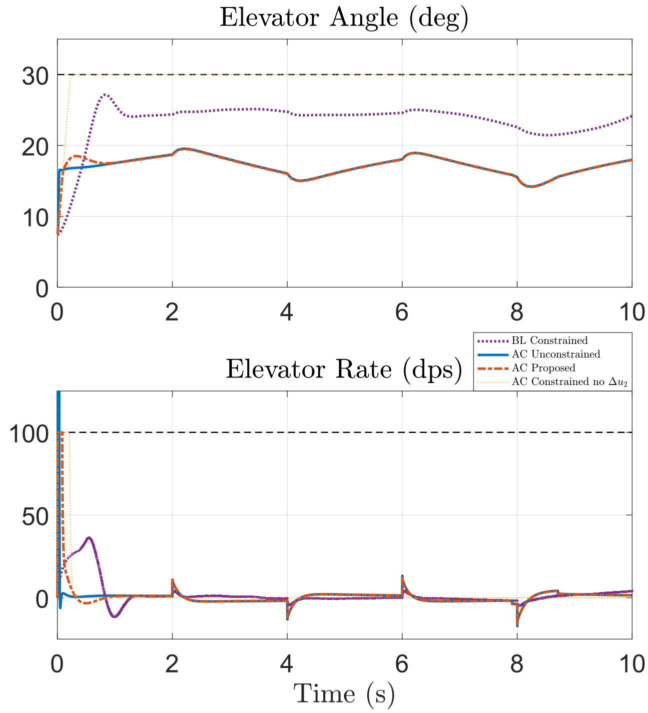


**FIGURE 10.** **High-speed vehicle. Longitudinal control magnitude and rate response comparison between baseline only control (BL Constrained), unconstrained adaptive control (AC Unconstrained), and constrained adaptive control with (AC Proposed) and without (AC Constrained no $\Delta u_2$) update law saturation modification.**

modified error model (38) and saturation update law (40), as described in this paper. In particular, AC proposed has a significantly improved pitch rate response as compared to the baseline controller. This improved response is due to the faster response of the control input as seen by the input rate profile in Figure 4. The AC proposed controller allows for significant performance recovery in the presence of the input limits. Figure 5 shows the integrated absolute value of the difference in pitch rate responses between the ideal not-limited adaptive control response and each of the baseline response and limited adaptive control response. In this figure the adaptive controller can be seen to provide for approximately half the integrated error. It should be noted that some accumulated error is expected given the constraints on the control input. Stability is maintained in the AC proposed controller by explicitly taking into account extra disturbance due to rate saturation as seen in Figure 5.

In order to demonstrate the effectiveness of the proposed adaptive controller for a MIMO system, with both magnitude and rate limits encountered, similar simulations were carried out for the lateral-directional subsystem of the numerical nonlinear F-16 simulation in Figures 6 and 7. In this simulation the aircraft experiences a 50% reduction in rolling moment coefficient $C_\ell$. The uncertainty results in a degradation in the performance of the roll rate response for the non-adaptive baseline controller as compared to the ideal unconstrained adaptive controller, as seen in Figure 8. The adaptive

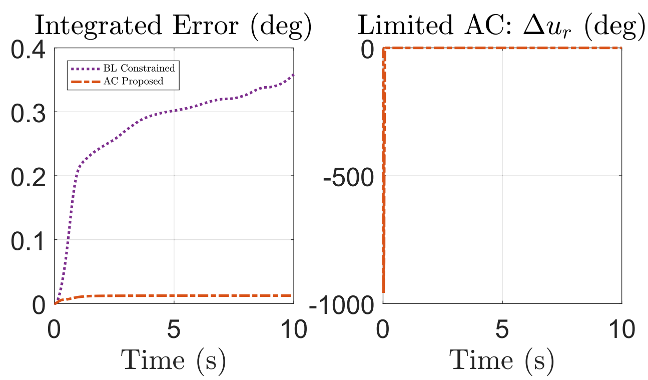


**FIGURE 11.** **High-speed vehicle. Left: Integral of the absolute value of the error between the ideal (unconstrained) adaptive control pitch rate response and the constrained baseline/proposed adaptive responses of Figure 9. Right: Time history of rate saturation elevator disturbance (13) for the proposed constrained adaptive controller with saturation modification.**

controller designed without the error model and update laws modified for the presence of input rate and magnitude limits can be seen to have a severely degraded response. In comparison, AC proposed closely recovers the ideal unconstrained response (up to the performance limits due to the input magnitude and rate constraints). In this simulation the effects of rate limits is even more apparent, where in Figure 7 it can be more clearly noticed that the limited adaptive control aileron angle response evolves linearly when an aileron rate limit is encountered. A comparison of the responses between the limited baseline and proposed adaptive controllers, along with a plot of the saturation disturbance $\Delta u_2$ for the proposed adaptive controller is shown in Figure 8.

### B. HIGH-SPEED VEHICLE NUMERICAL SIMULATION

This section provides numerical simulation results for an open loop unstable nonlinear high-speed vehicle model from [38], [39], [52], [53] in order to demonstrate the need for an output feedback adaptive controller capable of handling both rate limits and vehicle uncertainties, in the open loop unstable setting. This high-speed vehicle model is a blended wing/body aircraft driven by an air-breathing engine. The nonlinear high-speed vehicle model has aerodynamic forces and moments calculated from aerodynamic parameters based on flight condition. Numerous nonlinearities and unmeasured effects are present in this model due to the nonlinear high-speed vehicle dynamics and the uncertain changing aerodynamics of this model. Given that the longitudinal dynamics are open loop unstable, there is an even more significant need to counter uncertainties to restore tracking performance.

In order to obtain linearized dynamics for control design as in (5), a trim point was obtained at a straight and level flying condition. Similar to Section VI-A, the control design for the high-speed vehicle was separated into velocity, longitudinal and lateral-directional dynamics. In order to demonstrate uncertainty in the longitudinal dynamics, separate controllers were designed for the velocity and lateral-directional subsystems to maintain the trim condition in their respective subsystems. The requirement for an output feedback control solution is especially important in this example, as angle of attack sensors are infeasible.

As in [38], [39], [53], the longitudinal subsystem is stated as

$$x_p = \begin{bmatrix}\alpha & q\end{bmatrix}^\top \quad u_p = \delta_e \quad y_p = q \quad z_p = q,$$

where the longitudinal state is composed of the vehicle's angle of attack $\alpha$ and pitch rate $q$. Pitch rate is both the measured and regulated variable. An elevator deflection $\delta_e$ represents the input to the dynamics. The elevator gain parameter $\tau$ and saturation levels are as follows:

$$\tau = 0.02 \quad u_{\max} = \pm 30 \text{ deg} \quad u_{r,\max} = \pm 100 \text{ dps}.$$

In contrast to the F-16 simulation in the previous subsection, the longitudinal dynamics of this high-speed vehicle numerical simulation are open loop unstable. Once again, integral command tracking (6) was included in addition to the explicit inclusion of the dynamics of the magnitude and rate saturated actuator as in (14), resulting in complete plant models as in (15), (16) which satisfy Assumptions 1-3, as required.

Figures 9 and 10 show the response of the high-speed vehicle in the presence of a 50% decrease in the control effectiveness of all control surfaces and a shift in the center of gravity 0.1 ft rearward, with the pitch rate command stepped every two seconds. The uncertainty present in this simulation significantly degrades the ability of the non-adaptive baseline controller in (18) to track the desired pitch rate command. The angle of attack response of the baseline controller as seen in Figure 9 additionally becomes unacceptably large for a high-speed vehicle. This is another example of the motivation to employ an adaptive controller which is capable of countering the effects of uncertainty and restore the desired system response. In the absence of input limits, the adaptive control input, as in [33]–[37], and designed in (19) can be seen to result satisfactory command tracking in Figure 9 by the use of large control rates initially as seen in Figure 10. However, in the presence of input magnitude and rate limits, this controller can be seen to result in instability. The proposed adaptive controller which includes the modified error model (38), adaptive update law (40) and explicitly accounts for the presence of input magnitude and rate limits can be seen to result in a stable response which recovers the desired command tracking performance. Figure 11 shows the integrated absolute value of the error between the ideal unconstrained adaptive control response and each of the baseline response and the proposed adaptive control response. The baseline response performs significantly worse as compared to the proposed adaptive control response which explicitly accounts for input limits. The open loop unstable nature of the longitudinal dynamics of the high-speed vehicle results in a greater difference in the performance of the adaptive input limiter controller as compared to the baseline controller.

## VII. CONCLUSION

This paper presented the first MIMO adaptive architecture for controlling a plant model in the presence of parametric uncertainties with hard limits on both input magnitude and rate. The plant input is limited in both magnitude and rate through the use of a filter with hard saturation nonlinearities placed in the control path. Augmented adaptive update laws which explicitly account for the presence of the input limits were derived to provide for stable adaptation while in saturation. The stability analysis of signals in the closed-loop system is contained two parts: stable adaptation and bounded trajectories. The main result of stable adaptation and bounded trajectories greatly extends the current state-of-the-art in MIMO adaptive control in the presence of rate limits, as it provides a solution in output feedback form with hard saturation nonlinearities employed. The proposed controller was applied to a nonlinear numerical simulation of an open loop stable F-16 aircraft as well as a nonlinear numerical simulation of an open loop unstable high-speed vehicle. The MIMO simulations demonstrate successful input limiting, bounded trajectories, and the tracking performance of the adaptive controller presented in this paper.

## APPENDIX A CONSTANTS AND TIME-VARYING SCALARS

Throughout this paper the norm symbol $||X||$ denotes the 2-norm of element $X$.

### A. CONSTANT SCALARS

Define $P_B$ such that: $||\chi^\top(t)P_{cl}B_\Omega|| \leq P_B||\chi(t)||$
Define $P_C$ such that: $||\chi^\top(t)P_{cl}C_{\Delta\bar{u}_2}|| \leq P_C||\chi(t)||$
Define $P_Z$ such that: $||\chi^\top(t)P_{cl}B_z|| \leq P_Z||\chi(t)||$

$$\begin{aligned}
\gamma_{\max} &= \max\left[\text{eig}(\Gamma_\Omega), \text{eig}(\Gamma_{\Omega_\Delta})\right], \ \lambda_{\min} = \min(\text{eig}(\Lambda^*)) \\
u_{\min} &= \min_i(u_{\max,i}), \quad u_{r,\min} = \min_i(u_{r,\max,i}) \\
p_{\min} &= \min(\text{eig}(P_{cl})), \quad p_{\max} = \max(\text{eig}(P_{cl})) \\
\rho &= \sqrt{\frac{p_{\max}}{p_{\min}}}, \quad q_0 = \min(\text{eig}(Q_{cl})) \\
\tilde{\Omega}_{\max} &= \sup_t ||\tilde{\Omega}(t)|| \\
||B_{\xi,\Omega}|| &= (||\Omega^*|| + \tilde{\Omega}_{\max})||B_\xi|| \\
||K_{\xi,\Omega}|| &= (||\Omega^*|| + \tilde{\Omega}_{\max})||K_\xi|| \\
||K_{u_p}|| &= ||C_{u_p}||\left(||B_2\Lambda^* a_1^1||\left(\tilde{\Omega}_{\max}||C_{\bar{\xi}}||\right.\right. \\
&\qquad \left.\left. + (||\Omega^*|| + 1)\right) + 2\right) \\
\bar{\Omega}_{\max} &= \frac{q_0}{3P_B||C_{\bar{\xi}}||} \\
\kappa_1 &= 2P_C||S_C||\tilde{\Omega}_{\max}||\Gamma_C|| \\
\kappa_2 &= \left|-q_0 + 2\tilde{\Omega}_{\max}P_B||C_{\bar{\xi}}|| + 2P_C\frac{1}{a_1^1}||K_{\xi,\Omega}||\right| \\
\kappa_3 &= \alpha u_{\min} - \left(2P_Z + 2P_C\frac{1}{a_1^1}||B_{\xi,\Omega}||\right)z_{\text{cmd},\max} \\
\kappa_4 &= \tilde{\Omega}_{\max}^2\frac{a_1^1P_B||S_C||\cdot||\Gamma_C||\cdot||C_{\bar{\xi}}||}{||K_{\xi,\Omega}||} \\
\kappa_5 &= q_0 - 3\tilde{\Omega}_{\max}P_B||C_{\bar{\xi}}|| \\
\kappa_6 &= \left(2P_Z + \tilde{\Omega}_{\max}\frac{P_B||B_{\xi,\Omega}||\cdot||C_{\bar{\xi}}||}{||K_{\xi,\Omega}||}\right)z_{\text{cmd},\max} \\
\kappa_7 &= \left|-q_0 + 2\tilde{\Omega}_{\max}P_B||C_{\bar{\xi}}|| + \right. \\
&\qquad \left. 2P_C\frac{1}{a_1^1}\left(||K_{\xi,\Omega}|| + ||K_{u_p}||\right)\right| \\
\kappa_8 &= \beta u_{r,\min} - \left(2P_Z + 2P_C\frac{1}{a_1^1}||B_{\xi,\Omega}||\right)z_{\text{cmd},\max} \\
\kappa_9 &= \tilde{\Omega}_{\max}^2\frac{a_1^1P_B||S_C||\cdot||\Gamma_C||\cdot||C_{\bar{\xi}}||}{||K_{\xi,\Omega}|| + ||K_{u_p}||} \\
\kappa_{10} &= \left(2P_Z + \tilde{\Omega}_{\max}\frac{P_B||B_{\xi,\Omega}||\cdot||C_{\bar{\xi}}||}{||K_{\xi,\Omega}|| + ||K_{u_p}||}\right)z_{\text{cmd},\max} \\
\kappa_{11} &= 2P_Z z_{\text{cmd},\max} \\
\kappa_{12} &= q_0 - 2\tilde{\Omega}_{\max}P_B||C_{\bar{\xi}}||
\end{aligned}$$

$$\chi_{\min} = \max\left(\frac{\kappa_5 - \sqrt{\kappa_5^2 - 4\kappa_4\kappa_6}}{2\kappa_4}, \frac{\kappa_5 - \sqrt{\kappa_5^2 - 4\kappa_9\kappa_{10}}}{2\kappa_9}, \frac{\kappa_{11}}{\kappa_{12}}\right) \tag{54}$$

$$\chi_{\max} = \min\left(\frac{\sqrt{\kappa_2^2 + 4\kappa_1\kappa_3} - \kappa_2}{2\kappa_1}, \frac{\kappa_5 + \sqrt{\kappa_5^2 - 4\kappa_4\kappa_6}}{2\kappa_4}, \frac{\sqrt{\kappa_7^2 + 4\kappa_1\kappa_8} - \kappa_7}{2\kappa_1}, \frac{\kappa_5 + \sqrt{\kappa_5^2 - 4\kappa_9\kappa_{10}}}{2\kappa_9}\right) \tag{55}$$

Note that $\tilde{\Omega}_{\max} < \sqrt{\frac{V(0)\gamma_{\max}}{\lambda_{\min}}}$. Additionally, the ratio $\frac{q_0}{p_{\max}}$ is maximized with a choice of $Q_{cl} = I$ as seen in reference [54]. A bound on $\tilde{\Omega}$ may be enforced using the projection operator as is common in adaptive control [8]–[10].

### B. CONSTANT MATRICES

$$\begin{aligned}
A_{cl} &= \begin{bmatrix} -\frac{a_1^0}{a_1^1}I & \frac{1}{a_1^1}I & 0 & 0 \\ 0 & A - B_2K & LC & 0 \\ 0 & 0 & A_L^* & B_2^1\Lambda^* \\ 0 & 0 & 0 & -\frac{a_1^0}{a_1^1}I \end{bmatrix} \\
B_\Omega^\top &= \begin{bmatrix} 0 & 0 & (B_2^1\Lambda^*)^\top & 0 \end{bmatrix} \\
B_Z^\top &= \begin{bmatrix} 0 & B_z^\top & 0 & 0 \end{bmatrix} \\
B_\xi^\top &= \begin{bmatrix} 0 & a_1^1B_z^\top & 0 \end{bmatrix} \\
C_{\Delta\bar{u}_2}^\top &= \begin{bmatrix} 0 & 0 & 0 & I \end{bmatrix} \\
C_{u_p} &= \begin{bmatrix} 0 & \Lambda^{*-1} & 0 \end{bmatrix} \\
C_{\bar{\xi}} &= \begin{bmatrix} K & 0 & 0 & 0 \\ 0 & I & 0 & 0 \\ I & 0 & 0 & 0 \end{bmatrix} \\
K_\xi &= \begin{bmatrix} 0 & K & 0 & 0 \\ 0 & (a_1^0I + a_1^1(A - B_2K)) & a_1^1LC & 0 \\ 0 & I & 0 & 0 \end{bmatrix} \\
S_C &= S_2C \\
\Gamma_C &= C_{\bar{\xi}}^\top\Gamma_\Omega C_{\bar{\xi}}
\end{aligned}$$

### C. TIME-VARYING SCALARS

For ease of exposition, the following time varying scalars which represent the ratio of the saturated input magnitude and rate respectively to the unsaturated input magnitude and rate:

$$\mathbb{U} = \frac{||E_s(u(t), u_{\max})||}{||u(t)||}, \quad \mathbb{U}_r = \frac{||E_s(u_r(t), u_{r,\max})||}{||u_r(t)||}.$$

The magnitude of the computed control input (19) may be expressed as

$$||u(t)|| = ||(a_1^1s + a_1^0)\Omega^\top(t)\bar{\xi}(t)||$$

$$\begin{aligned}
&= ||\Omega^\top(t)(a_1^1 s + a_1^0)\bar{\xi}(t) + a_1^1\dot{\Omega}^\top(t)\bar{\xi}(t)|| \\
&= || - \Omega^\top(t)K_\xi\chi(t) - \Omega^\top(t)B_\xi z_{\text{cmd}}(t) \\
&\quad - a_1^1 S_2 Ce_{mu}(t)\chi^\top(t)\Gamma_C\chi(t)|| \\
&\leq ||K_{\xi,\Omega}|| \cdot ||\chi(t)|| + ||B_{\xi,\Omega}||z_{\text{cmd,max}} \\
&\quad + a_1^1||S_C||\tilde{\Omega}_{\max}||\Gamma_C|| \cdot ||\chi(t)||^2. \qquad (56)
\end{aligned}$$

The magnitude of the plant input may be expressed as follows, through applying equation (30):

$$\begin{aligned}
||u_p(t)|| &= ||C_{u_p}(e_x(t) + x_m(t))|| \\
&= ||C_{u_p}(B_2\Lambda^* a_1^1\Big[\bar{\Psi}_2^{*\top}\bar{x}_m(t) + \Omega^\top(t)\bar{\xi}(t) \\
&\quad - \Lambda^{*-1}\bar{u}_{bl}(t) + \Delta\bar{u}_2(t)\Big] + e_{mx}(t) + x_m(t))|| \\
&\leq ||K_{u_p}|| \cdot ||\chi(t)||. \qquad (57)
\end{aligned}$$

Additionally, from equation (12) the following holds:

$$||u_r(t)|| \leq \frac{1}{\tau}\left(||u(t)|| + ||u_p(t)||\right) \qquad (58)$$

## APPENDIX B PROOF OF THEOREM 1, STEP 2

### A. $\Delta u = 0, \Delta u_r = 0$

In this case (47) can be simplified as

$$\dot{\chi}(t) = A_{cl}\chi(t) - B_\Omega\tilde{\Omega}^\top(t)C_{\bar{\xi}}\chi(t) + B_Z z_{\text{cmd}}(t).$$

This leads to the following time derivative of the candidate Lyapunov function in equation (49):

$$\begin{aligned}
\dot{W}(\chi(t)) &= -\chi^\top(t)Q_{cl}\chi(t) - 2\chi^\top(t)P_{cl}B_\Omega\tilde{\Omega}^\top(t)C_{\bar{\xi}}\chi(t) \\
&\quad + 2\chi^\top(t)P_{cl}B_Z z_{\text{cmd}}(t).
\end{aligned}$$

The right hand side may be bounded as

$$\begin{aligned}
\dot{W}(\chi(t)) &\leq -\left(q_0 - 2\tilde{\Omega}_{\max}P_B||C_{\bar{\xi}}||\right)||\chi(t)||^2 \\
&\quad + \left(2P_Z z_{\text{cmd,max}}\right)||\chi(t)||.
\end{aligned}$$

Using the definition of $\tilde{\Omega}_{\max}$ and condition $(ii)$ of Theorem 1, implies $\dot{W}(\chi(t)) < 0$, for $||\chi(t)|| > \frac{\kappa_{11}}{\kappa_{12}}$. Choosing $\chi_{\min}$ from equation (54) implies

$$\dot{W}(\chi(t)) < 0, \quad \forall\chi(t) \in \mathcal{A} \text{ in case A.} \qquad (59)$$

### B. $\Delta u \neq 0, \Delta u_r = 0$

In this case (47) can be rewritten as

$$\begin{aligned}
\dot{\chi}(t) &= A_{cl}\chi(t) - B_\Omega\tilde{\Omega}^\top(t)C_{\bar{\xi}}\chi(t) \\
&\quad + C_{\Delta\bar{u}_2}\frac{1}{a_1^1}\left(\mathbb{U} - 1\right)u(t) + B_Z z_{\text{cmd}}(t).
\end{aligned}$$

This leads to the following time derivative of the candidate Lyapunov function in equation (49):

$$\begin{aligned}
\dot{W}(\chi(t)) = &- \chi^\top(t)Q_{cl}\chi(t) - 2\chi^\top(t)P_{cl}B_\Omega\tilde{\Omega}^\top(t)C_{\bar{\xi}}\chi(t) \\
&+ 2\chi^\top(t)P_{cl}C_{\Delta\bar{u}_2}\frac{1}{a_1^1}\left(\mathbb{U} - 1\right)u(t) \\
&+ 2\chi^\top(t)P_{cl}B_Z z_{\text{cmd}}(t).
\end{aligned}$$

Three sub-cases are considered in this section.

#### 1) SUB-CASE I

$$2\chi^\top(t)P_{cl}C_{\Delta\bar{u}_2}\frac{1}{a_1^1}\mathbb{U}u(t) < -\alpha u_{\min}||\chi(t)||$$

The time derivative of the candidate Lyapunov function may be bounded using the condition of this sub-case and (56) as

$$\begin{aligned}
\dot{W}(\chi(t)) &\leq \left(2P_C||S_C||\tilde{\Omega}_{\max}||\Gamma_C||\right)||\chi(t)||^3 \\
&+ \left(-q_0 + 2\tilde{\Omega}_{\max}P_B||C_{\bar{\xi}}|| + 2P_C\frac{1}{a_1^1}||K_{\xi,\Omega}||\right)||\chi(t)||^2 \\
&- \left(\alpha u_{\min} - (2P_Z + 2P_C\frac{1}{a_1^1}||B_{\xi,\Omega}||)z_{\text{cmd,max}}\right)||\chi(t)||.
\end{aligned}$$

Thus: $\dot{W}(\chi(t)) < 0$, for $||\chi(t)|| < \frac{\sqrt{\kappa_2^2 + 4\kappa_1\kappa_3} - \kappa_2}{2\kappa_1}$. Choosing $\chi_{\max}$ from equation (55) implies

$$\dot{W}(\chi(t)) < 0, \quad \forall\chi(t) \in \mathcal{A} \text{ in case B, sub-case } (i). \qquad (60)$$

#### 2) SUB-CASE II

$$0 > 2\chi^\top(t)P_{cl}C_{\Delta\bar{u}_2}\frac{1}{a_1^1}\mathbb{U}u(t) > -\alpha u_{\min}||\chi(t)||$$

The condition of this sub-case implies

$$0 < 2\chi^\top(t)P_{cl}C_{\Delta\bar{u}_2}\frac{1}{a_1^1}\mathbb{U}u(t) + \alpha u_{\min}||\chi(t)||.$$

Apply $\frac{u_{\min}}{||E_s(u(t), u_{\max})||} \leq 1$:

$$0 < 2\chi^\top(t)P_{cl}C_{\Delta\bar{u}_2}\frac{1}{a_1^1}u(t) + \alpha||u(t)|| \cdot ||\chi(t)||.$$

Add terms to create $\dot{W}(\chi(t))$ on the left hand side:

$$\begin{aligned}
\dot{W}(\chi(t)) &< -\chi^\top(t)Q_{cl}\chi(t) - 2\chi^\top(t)P_{cl}B_\Omega\tilde{\Omega}^\top(t)C_{\bar{\xi}}\chi(t) \\
&\quad + 2\chi^\top(t)P_{cl}C_{\Delta\bar{u}_2}\frac{1}{a_1^1}\left(\mathbb{U} - 1\right)u(t) \\
&\quad + 2\chi^\top(t)P_{cl}B_Z z_{\text{cmd}}(t) \\
&\quad + 2\chi^\top(t)P_{cl}C_{\Delta\bar{u}_2}\frac{1}{a_1^1}u(t) \\
&\quad + \alpha||u(t)|| \cdot ||\chi(t)||.
\end{aligned}$$

Apply the case inequality, $0 > 2\chi^\top(t)P_{cl}C_{\Delta\bar{u}_2}\frac{1}{a_1^1}\mathbb{U}u(t)$:

$$\begin{aligned}
\dot{W}(\chi(t)) &< -\chi^\top(t)Q_{cl}\chi(t) - 2\chi^\top(t)P_{cl}B_\Omega\tilde{\Omega}^\top(t)C_{\bar{\xi}}\chi(t) \\
&\quad + \alpha||u(t)|| \cdot ||\chi(t)|| + 2\chi^\top(t)P_{cl}B_Z z_{\text{cmd}}(t).
\end{aligned}$$

Apply (56):

$$\begin{aligned}
\dot{W}(\chi(t)) < &- \chi^\top(t)Q_{cl}\chi(t) - 2\chi^\top(t)P_{cl}B_\Omega\tilde{\Omega}^\top(t)C_{\bar{\xi}}\chi(t) \\
&+ \alpha||K_{\xi,\Omega}|| \cdot ||\chi(t)||^2 \\
&+ \alpha||B_{\xi,\Omega}||z_{\text{cmd,max}}||\chi(t)|| \\
&+ \alpha a_1^1||S_C||\tilde{\Omega}_{\max}||\Gamma_C|| \cdot ||\chi(t)||^3 \\
&+ 2\chi^\top(t)P_{cl}B_Z z_{\text{cmd}}(t).
\end{aligned}$$

Maximize the right hand side:

$$\begin{aligned}\dot{W}(\chi(t)) < &\left(\alpha a_1^1 ||S_C|| |\tilde{\Omega}_{\max}||\Gamma_C||\right) ||\chi(t)||^3 \\ &- \left(q_0 - 2P_B\tilde{\Omega}_{\max}||C_{\bar{\xi}}|| - \alpha||K_{\xi,\Omega}||\right) ||\chi(t)||^2 \\ &+ \left((2P_Z + \alpha||B_{\xi,\Omega}||)z_{\text{cmd,max}}\right) ||\chi(t)||.\end{aligned}$$

Apply $\alpha = \frac{P_B\tilde{\Omega}_{\max}||C_{\bar{\xi}}||}{||K_{\xi,\Omega}||}$:

$$\begin{aligned}\dot{W}(\chi(t)) < &\left(\tilde{\Omega}^2_{\max}\frac{a_1^1 P_B||S_C||\cdot||\Gamma_C||\cdot||C_{\bar{\xi}}||}{||K_{\xi,\Omega}||}\right)||\chi(t)||^3 \\ &- \left(q_0 - 3\tilde{\Omega}_{\max}P_B||C_{\bar{\xi}}||\right)||\chi(t)||^2 \\ &+ \left(\left(2P_Z + \tilde{\Omega}_{\max}\frac{P_B||B_{\xi,\Omega}||\cdot||C_{\bar{\xi}}||}{||K_{\xi,\Omega}||}\right)\right. \\ &\left.\times z_{\text{cmd,max}}\right)||\chi(t)||.\end{aligned}$$

Using the definition of $\tilde{\Omega}_{\max}$ and condition (*ii*) of Theorem 1, implies $\dot{W}(\chi(t)) < 0$ for

$$\frac{\kappa_5 - \sqrt{\kappa_5^2 - 4\kappa_4\kappa_6}}{2\kappa_4} < ||\chi(t)|| < \frac{\kappa_5 + \sqrt{\kappa_5^2 - 4\kappa_4\kappa_6}}{2\kappa_4}.$$

Choosing $\chi_{\min}$, $\chi_{\max}$ from equations (54) and (55) implies

$$\dot{W}(\chi(t)) < 0, \quad \forall\chi(t) \in \mathcal{A} \text{ in case B, sub-case } (ii). \quad (61)$$

### 3) SUB-CASE III

$$2\chi^\top(t)P_{cl}C_{\Delta\bar{u}_2}\frac{1}{a_1^1}\mathbb{U}u(t) > 0$$

The condition of this sub-case implies the following:

$$2\chi^\top(t)P_{cl}C_{\Delta\bar{u}_2}\frac{1}{a_1^1}\mathbb{U}u(t) < 2\chi^\top(t)P_{cl}C_{\Delta\bar{u}_2}\frac{1}{a_1^1}u(t).$$

Add terms to create $\dot{W}(\chi(t))$ on the left hand side:

$$\begin{aligned}\dot{W}(\chi(t)) \leq &-\chi^\top(t)Q_{cl}\chi(t) - 2\chi^\top(t)P_{cl}B_\Omega\tilde{\Omega}^\top(t)C_{\bar{\xi}}\chi(t) \\ &+ 2\chi^\top(t)P_{cl}B_Z z_{\text{cmd}}(t).\end{aligned}$$

The right hand side may be maximized as

$$\begin{aligned}\dot{W}(\chi(t)) \leq &-\left(q_0 - 2\tilde{\Omega}_{\max}P_B||C_{\bar{\xi}}||\right)||\chi(t)||^2 \\ &+ \left(2P_Z z_{\text{cmd,max}}\right)||\chi(t)||.\end{aligned}$$

Using the definition of $\tilde{\Omega}_{\max}$ and condition (*ii*) of Theorem 1, implies $\dot{W}(\chi(t)) < 0$, for $||\chi(t)|| > \frac{\kappa_{11}}{\kappa_{12}}$. Choosing $\chi_{\min}$ from equation (54) implies

$$\dot{W}(\chi(t)) < 0, \quad \forall\chi(t) \in \mathcal{A} \text{ in case B, sub-case } (iii). \quad (62)$$

## C. $\Delta u = 0$, $\Delta u_r \neq 0$

In this case (47) can be rewritten as

$$\begin{aligned}\dot{\chi}(t) = &A_{cl}\chi(t) - B_\Omega\tilde{\Omega}^\top(t)C_{\bar{\xi}}\chi(t) \\ &+ C_{\Delta\bar{u}_2}\frac{1}{a_1^1}\left(\mathbb{U}_r - 1\right)\tau u_r(t) + B_Z z_{\text{cmd}}(t).\end{aligned}$$

The following is the time derivative of the candidate Lyapunov function in equation (49):

$$\begin{aligned}\dot{W}(\chi(t)) = &-\chi^\top(t)Q_{cl}\chi(t) - 2\chi^\top(t)P_{cl}B_\Omega\tilde{\Omega}^\top(t)C_{\bar{\xi}}\chi(t) \\ &+ 2\chi^\top(t)P_{cl}C_{\Delta\bar{u}_2}\frac{1}{a_1^1}\left(\mathbb{U}_r - 1\right)\tau u_r(t) \\ &+ 2\chi^\top(t)P_{cl}B_Z z_{\text{cmd}}(t).\end{aligned}$$

Three sub-cases are considered in this section.

### 1) SUB-CASE I

$$2\chi^\top(t)P_{cl}C_{\Delta\bar{u}_2}\frac{1}{a_1^1}\mathbb{U}_r\tau u_r(t) < -\beta u_{r,\min}||\chi(t)||$$

The time derivative of the candidate Lyapunov function may be bounded using the condition of this sub-case and (58) as

$$\begin{aligned}\dot{W}(\chi(t)) \leq &\left(2P_C||S_C|| |\tilde{\Omega}_{\max}||\Gamma_C||\right)||\chi(t)||^3 \\ &+ \left(-q_0 + 2\tilde{\Omega}_{\max}P_B||C_{\bar{\xi}}||\right. \\ &\left.+ 2P_C\frac{1}{a_1^1}\left(||K_{\xi,\Omega}|| + ||K_{u_p}||\right)\right)||\chi(t)||^2 \\ &- \left(\beta u_{r,\min} - (2P_Z + \frac{2P_C}{a_1^1}||B_{\xi,\Omega}||)z_{\text{cmd,max}}\right)||\chi(t)||.\end{aligned}$$

Thus: $\dot{W}(\chi(t)) < 0$, for $||\chi(t)|| < \frac{\sqrt{\kappa_7^2 + 4\kappa_1\kappa_8} - \kappa_7}{2\kappa_1}$. Choosing $\chi_{\max}$ from equation (55) implies

$$\dot{W}(\chi(t)) < 0, \quad \forall\chi(t) \in \mathcal{A} \text{ in case C, sub-case } (i). \quad (63)$$

### 2) SUB-CASE II

$$0 > 2\chi^\top(t)P_{cl}C_{\Delta\bar{u}_2}\frac{1}{a_1^1}\mathbb{U}_r\tau u_r(t) > -\beta u_{r,\min}||\chi(t)||$$

The condition of this sub-case implies

$$0 < 2\chi^\top(t)P_{cl}C_{\Delta\bar{u}_2}\frac{1}{a_1^1}\mathbb{U}_r\tau u_r(t) + \beta u_{r,\min}||\chi(t)||.$$

Apply $\frac{u_{r,\min}}{||E_s(u_r(t),u_{r,\max})||} \leq 1$:

$$0 < 2\chi^\top(t)P_{cl}C_{\Delta\bar{u}_2}\frac{1}{a_1^1}\tau u_r(t) + \beta||u_r(t)||\cdot||\chi(t)||.$$

Add terms to create $\dot{W}(\chi(t))$ on the left hand side:

$$\begin{aligned}\dot{W}(\chi(t)) < &-\chi^\top(t)Q_{cl}\chi(t) - 2\chi^\top(t)P_{cl}B_\Omega\tilde{\Omega}^\top(t)C_{\bar{\xi}}\chi(t) \\ &+ 2\chi^\top(t)P_{cl}C_{\Delta\bar{u}_2}\frac{1}{a_1^1}\left(\mathbb{U}_r - 1\right)\tau u_r(t) \\ &+ 2\chi^\top(t)P_{cl}B_Z z_{\text{cmd}}(t) \\ &+ 2\chi^\top(t)P_{cl}C_{\Delta\bar{u}_2}\frac{1}{a_1^1}\tau u_r(t) \\ &+ \beta||u_r(t)||\cdot||\chi(t)||.\end{aligned}$$

Apply the case inequality, $0 > 2\chi^\top(t)P_{cl}C_{\Delta\bar{u}_2}\frac{1}{a_1^1}\mathbb{U}_r\tau u_r(t)$:

$$\dot{W}(\chi(t)) < -\chi^\top(t)Q_{cl}\chi(t) - 2\chi^\top(t)P_{cl}B_\Omega\tilde{\Omega}^\top(t)C_\xi\chi(t) + \beta||u_r(t)||\cdot||\chi(t)|| + 2\chi^\top(t)P_{cl}B_Z z_{\text{cmd}}(t).$$

Apply (56), (57), and (58):

$$\begin{aligned}\dot{W}(\chi(t)) < {} & -\chi^\top(t)Q_{cl}\chi(t) - 2\chi^\top(t)P_{cl}B_\Omega\tilde{\Omega}^\top(t)C_\xi\chi(t) \\ & + \frac{\beta}{\tau}\left(||K_{\xi,\Omega}|| + ||K_{u_p}||\right)||\chi(t)||^2 \\ & + \frac{\beta}{\tau}||B_{\xi,\Omega}||z_{\text{cmd,max}}||\chi(t)|| \\ & + \frac{\beta}{\tau}a_1^1||S_C||\tilde{\Omega}_{\max}||\Gamma_C||\cdot||\chi(t)||^3 \\ & + 2\chi^\top(t)P_{cl}B_Z z_{\text{cmd}}(t).\end{aligned}$$

Maximize the right hand side:

$$\begin{aligned}\dot{W}(\chi(t)) < {} & \left(\frac{\beta}{\tau}a_1^1||S_C||\tilde{\Omega}_{\max}||\Gamma_C||\right)||\chi(t)||^3 \\ & + \Big(-q_0 + 2P_B\tilde{\Omega}_{\max}||C_\xi|| \\ & + \frac{\beta}{\tau}\left(||K_{\xi,\Omega}|| + ||K_{u_p}||\right)\Big)||\chi(t)||^2 \\ & + \left(\left(2P_Z + \frac{\beta}{\tau}||B_{\xi,\Omega}||\right)z_{\text{cmd,max}}\right)||\chi(t)||.\end{aligned}$$

Apply $\beta = \frac{\tau P_B\tilde{\Omega}_{\max}||C_\xi||}{||K_{\xi,\Omega}|| + ||K_{u_p}||}$:

$$\begin{aligned}\dot{W}(\chi(t)) < {} & \left(\tilde{\Omega}^2_{\max}\frac{a_1^1P_B||S_C||\cdot||\Gamma_C||\cdot||C_\xi||}{||K_{\xi,\Omega}|| + ||K_{u_p}||}\right)||\chi(t)||^3 \\ & - \left(q_0 - 3\tilde{\Omega}_{\max}P_B||C_\xi||\right)||\chi(t)||^2 \\ & + \Bigg(\left(2P_Z + \tilde{\Omega}_{\max}\frac{P_B||B_{\xi,\Omega}||\cdot||C_\xi||}{||K_{\xi,\Omega}|| + ||K_{u_p}||}\right) \\ & \times z_{\text{cmd,max}}\Bigg)||\chi(t)||.\end{aligned}$$

Using the definition of $\tilde{\Omega}_{\max}$ and condition (*ii*) of Theorem 1, implies $\dot{W}(\chi(t)) < 0$ for

$$\frac{\kappa_5 - \sqrt{\kappa_5^2 - 4\kappa_9\kappa_{10}}}{2\kappa_9} < ||\chi(t)|| < \frac{\kappa_5 + \sqrt{\kappa_5^2 - 4\kappa_9\kappa_{10}}}{2\kappa_9}.$$

Choosing $\chi_{\min}, \chi_{\max}$ from equations (54) and (55) implies

$$\dot{W}(\chi(t)) < 0, \quad \forall\chi(t) \in \mathcal{A} \text{ in case C, sub-case } (ii). \quad (64)$$

### 3) SUB-CASE III

$$2\chi^\top(t)P_{cl}C_{\Delta\bar{u}_2}\frac{1}{a_1^1}\mathbb{U}_r\tau u_r(t) > 0$$

The condition of this sub-case implies the following:

$$2\chi^\top(t)P_{cl}C_{\Delta\bar{u}_2}\frac{1}{a_1^1}\mathbb{U}_r\tau u_r(t) < 2\chi^\top(t)P_{cl}C_{\Delta\bar{u}_2}\frac{1}{a_1^1}\tau u_r(t).$$

Add terms to create $\dot{W}(\chi(t))$ on the left hand side:

$$\dot{W}(\chi(t)) \le -\chi^\top(t)Q_{cl}\chi(t) - 2\chi^\top(t)P_{cl}B_\Omega\tilde{\Omega}^\top(t)C_\xi\chi(t) + 2\chi^\top(t)P_{cl}B_Z z_{\text{cmd}}(t).$$

The right hand side may be maximized as:

$$\dot{W}(\chi(t)) \le -\left(q_0 - 2\tilde{\Omega}_{\max}P_B||C_\xi||\right)||\chi(t)||^2 + \left(2P_Z z_{\text{cmd,max}}\right)||\chi(t)||.$$

Using the definition of $\tilde{\Omega}_{\max}$ and condition (*ii*) of Theorem 1, implies $\dot{W}(\chi(t)) < 0$, for $||\chi(t)|| > \frac{\kappa_{11}}{\kappa_{12}}$. Choosing $\chi_{\min}$ from equation (54) implies

$$\dot{W}(\chi(t)) < 0, \quad \forall\chi(t) \in \mathcal{A} \text{ in case C, sub-case } (iii). \quad (65)$$

From equations (59), (60), (61), (62), (63), (64), (65) it can be concluded that

$$\dot{W}(\chi(t)) < 0, \quad \forall\chi(t) \in \mathcal{A}. \quad (66)$$

## ACKNOWLEDGMENT

The authors would like to thank Dr. Daniel Wiese for providing useful numerical simulation scripts.

## REFERENCES

[1] J. Sofrony, M. C. Turner, I. Postlethwaite, O. Brieger, and D. Leibling, "Anti-windup synthesis for PIO avoidance in an experimental aircraft," in *Proc. 45th IEEE Conf. Decis. Control*, Dec. 2006, pp. 5412–5417.
[2] H. Duda, "Effects of rate limiting elements in flight control systems—A new PIO-criterion," in *Proc. Guid., Navigat., Control Conf.*, Aug. 1995, p. 3204.
[3] F. Amato, R. Iervolino, M. Pandit, S. Scala, and L. Verde, "Analysis of pilot-in-the-loop oscillations due to position and rate saturations," in *Proc. 39th IEEE Conf. Decis. Control*, Dec. 2000, pp. 3564–3569.
[4] L. Rundqwist and K. Stahl-Gunnarsson, "Phase compensation of rate limiters in unstable aircraft," in *Proc. IEEE Int. Conf. Control Appl., IEEE Int. Conf. Control Appl. Held Together, IEEE Int. Symp. Intell. Contro*, Sep. 1996, pp. 19–24.
[5] L. Rundqwist and R. Hillgren, "Phase compensation of rate limiters in JAS 39 gripen," in *Proc. 21st Atmos. Flight Mech. Conf.*, Jul. 1996, p. 3368.
[6] S. Sastry and M. Bodson, *Adaptive Control: Stability, Convergence and Robustness*. Hoboken, NJ, USA: Prentice-Hall, 1989.
[7] K. J. Åström and B. Wittenmark, *Adaptive Control*, 2nd ed. Boston, MA, USA: Addison-Wesley, 1995.
[8] P. A. Ioannou and J. Sun, *Robust Adaptive Control*. Hoboken, NJ, USA: Prentice-Hall, 1996.
[9] K. S. Narendra and A. M. Annaswamy, *Stable Adaptive Systems*. Hoboken, NJ, USA: Prentice-Hall, 2005.
[10] E. Lavretsky and K. A. Wise, *Robust and Adaptive Control With Aerospace Applications*. Berlin, Germany: Springer, 2013.
[11] N. T. Nguyen, *Model-Reference Adaptive Control*. Berlin, Germany: Springer, 2018.
[12] S. P. Karason and A. M. Annaswamy, "Adaptive control in the presence of input constraints," *IEEE Trans. Autom. Control*, vol. 39, no. 11, pp. 2325–2330, Nov. 1994.
[13] A. M. Annaswamy and S. P. Karason, "Discrete-time adaptive control in the presence of input constraints," *Automatica*, vol. 31, no. 10, pp. 1421–1431, 1995.
[14] M. Schwager, "Towards verifiable adaptive control for safety critical applications," M.S. thesis, Dept. Mech. Eng., MIT, Cambridge, MA, USA, 2005.
[15] J. Jang, "Adaptive control design with guaranteed margins for nonlinear plants," Ph.D. dissertation, Dept. Mech. Eng., MIT, Cambridge, MA, USA, 2009.
[16] E. Lavretsky and N. Hovakimyan, "Stable adaptation in the presence of actuator constraints with flight control applications," *J. Guid. Control Dyn.*, vol. 30, no. 2, pp. 337–345, Mar. 2007.

[17] A. Serrani, A. M. Zinnecker, L. Fiorentini, M. A. Bolender, and D. B. Doman, "Integrated adaptive guidance and control of constrained nonlinear air-breathing hypersonic vehicle models," in *Proc. Amer. Control Conf.*, Jun. 2009, pp. 3172–3177.

[18] B. C. Gruenwald, S. B. Sarsilmaz, T. Yucelen, and J. A. Muse, "A new model reference adaptive control law to address actuator amplitude saturation," in *Proc. AIAA Scitech Forum*, Jan. 2019, p. 1424.

[19] B. C. Gruenwald, T. Yucelen, K. M. Dogan, and J. A. Muse, "On adaptive control of uncertain dynamical systems in the presence of actuator dynamics and amplitude saturation limits," in *Proc. Amer. Control Conf. (ACC)*, Jul. 2019, pp. 423–428.

[20] Q. M. Lam, D. T. Drake, and D. B. Ridgely, "Input saturation treatments: A performance comparison of direct adaptive control and $\theta$—D control methodologies," in *Proc. IEEE Aerosp. Conf.*, Mar. 2007, pp. 1–15.

[21] R. A. Hess and S. A. Snell, "Flight control system design with rate saturating actuators," *J. Guid. Control Dyn.*, vol. 20, no. 1, pp. 90–96, Jan. 1997.

[22] C. Barbu, S. Galeani, A. R. Teel, and L. Zaccarian, "Non-linear anti-windup for manual flight control," *Int. J. Control*, vol. 78, no. 14, pp. 1111–1129, Sep. 2005.

[23] S. Galeani, S. Onori, A. R. Teel, and L. Zaccarian, "A magnitude and rate saturation model and its use in the solution of a static anti-windup problem," *Syst. Control Lett.*, vol. 57, no. 1, pp. 1–9, Jan. 2008.

[24] N. E. Kahveci and P. A. Ioannou, "Indirect adaptive control for systems with input rate saturation," in *Proc. Amer. Control Conf.*, Jun. 2008, pp. 3396–3401.

[25] M. Matsutani, A. Annaswamy, and L. Crespo, "Adaptive control in the presence of rate saturation with application to a transport aircraft model," in *Proc. AIAA Guid., Navigat., Control Conf.*, Aug. 2010, p. 7771.

[26] K. J. Astrom and L. Rundqwist, "Integrator windup and how to avoid it," in *Proc. Amer. Control Conf.*, Jun. 1989, pp. 1693–1698.

[27] K. J. Astrom and B. Wittenmark, *Adaptive Control*, 2nd ed. New York, NY, USA: Dover, 2008.

[28] A. Leonessa, W. M. Haddad, T. Hayakawa, and Y. Morel, "Adaptive control for nonlinear uncertain systems with actuator amplitude and rate saturation constraints," *Int. J. Adapt. Control Signal Process.*, vol. 23, no. 1, pp. 73–96, 2009.

[29] M. Chen, S. S. Ge, and B. V. E. How, "Robust adaptive neural network control for a class of uncertain MIMO nonlinear systems with input nonlinearities," *IEEE Trans. Neural Netw.*, vol. 21, no. 5, pp. 796–812, May 2010.

[30] M. Chen, S. S. Ge, and B. Ren, "Adaptive tracking control of uncertain MIMO nonlinear systems with input constraints," *Automatica*, vol. 47, no. 3, pp. 452–465, Mar. 2011.

[31] J. E. Gaudio, A. M. Annaswamy, and E. Lavretsky, "Adaptive control of hypersonic vehicles in the presence of rate limits," in *Proc. AIAA Guid., Navigat., Control Conf.*, Jan. 2018, p. 0846.

[32] J. E. Gaudio, "Fast learning and adaptation in control and machine learning," Ph.D. dissertation, Dept. Mech. Eng., MIT, Cambridge, MA, USA, 2020.

[33] Z. Qu, E. Lavretsky, and A. M. Annaswamy, "An adaptive controller for very flexible aircraft," in *Proc. AIAA Guid., Navigat., Control (GNC) Conf.*, Aug. 2013, p. 4854.

[34] Z. Qu, A. M. Annaswamy, and E. Lavretsky, "Adaptive output-feedback control for relative degree two systems based on closed-loop reference models," in *Proc. 54th IEEE Conf. Decis. Control (CDC)*, Dec. 2015, pp. 7598–7603.

[35] Z. Qu, A. M. Annaswamy, and E. Lavretsky, "Adaptive output-feedback control for a class of multi-input-multi-output plants with applications to very flexible aircraft," in *Proc. Amer. Control Conf. (ACC)*, Jul. 2016, pp. 1613–1618.

[36] Z. Qu, "Adaptive output-feedback control and applications to very flexible aircraft," Ph.D. dissertation, Dept. Mech. Eng., MIT, Cambridge, MA, USA, 2016.

[37] Z. Qu, B. T. Thomsen, and A. M. Annaswamy, "Adaptive control for a class of multi-input multi-output plants with arbitrary relative degree," *IEEE Trans. Autom. Control*, vol. 65, no. 7, pp. 3023–3038, Jul. 2020.

[38] D. P. Wiese, A. M. Annaswamy, J. A. Muse, M. A. Bolender, and E. Lavretsky, "Adaptive output feedback based on closed-loop reference models for hypersonic vehicles," *J. Guid., Control, Dyn.*, vol. 38, no. 12, pp. 2429–2440, May 2015.

[39] D. P. Wiese, A. M. Annaswamy, J. A. Muse, M. A. Bolender, and E. Lavretsky, "Sequential loop closure based adaptive output feedback," *IEEE Access*, vol. 5, pp. 23436–23451, 2017.

[40] K. A. Wise, "Design parameter tuning in adaptive observer-based flight control architectures," in *Proc. Inf. Syst.-AIAA Infotech Aerosp.*, Jan. 2018, p. 0248.

[41] E. Lavretsky, "Design, analysis, and flight evaluation of a primary control system with observer-based loop transfer recovery and direct adaptive augmentation for the calspan variable stability simulator learjet-25B aircraft," in *Proc. AIAA Scitech Forum*, Jan. 2019, p. 1081.

[42] E. Lavretsky, "Adaptive output feedback design using asymptotic properties of LQG/LTR controllers," *IEEE Trans. Autom. Control*, vol. 57, no. 6, pp. 1587–1591, Jun. 2012.

[43] K. A. Wise and E. Lavretsky, "Flight control design using observer-based loop transfer recovery," in *Proc. AIAA Guid., Navigat., Control (GNC) Conf.*, Aug. 2013, p. 5105.

[44] T. Gibson, A. Annaswamy, and E. Lavretsky, "Improved transient response in adaptive control using projection algorithms and closed loop reference models," in *Proc. AIAA Guid., Navigat., Control Conf.*, Aug. 2012, p. 4775.

[45] T. E. Gibson, A. M. Annaswamy, and E. Lavretsky, "Adaptive systems with closed-loop reference-models, Part I: Transient performance," in *Proc. Amer. Control Conf.*, Jun. 2013, pp. 3376–3383.

[46] T. E. Gibson, A. M. Annaswamy, and E. Lavretsky, "On adaptive control with closed-loop reference models: Transients, oscillations, and peaking," *IEEE Access*, vol. 1, pp. 703–717, 2013.

[47] T. E. Gibson, "Closed-loop reference model adaptive control: With application to very flexible aircraft," Ph.D. dissertation, Dept. Mech. Eng., MIT, Cambridge, MA, USA, 2014.

[48] W. E. Schmitendorf and B. R. Barmish, "Null controllability of linear systems with constrained controls," *SIAM J. Control Optim.*, vol. 18, no. 4, pp. 327–345, Jul. 1980.

[49] B. L. Stevens and F. L. Lewis, *Aircraft Control and Simulation*. Hoboken, NJ, USA: Wiley, 2003.

[50] R. S. Russell, "Non-linear F-16 simulation using simulink and MATLAB," Univ. Minnesota, Minneapolis, MN, USA, Tech. Rep., 2003. [Online]. Available: http://www.aem.umn.edu/~balas/darpa_sec/software/F16Manual.pdf

[51] L. T. Nguyen, M. E. Ogburn, W. P. Gilbert, K. S. Kibler, P. W. Brown, and P. L. Deal, "Simulator study of stall/post-stall characteristics of a fighter airplane with relaxed longitudinal static stability," NASA, Washington, DC, USA, Tech. Rep. 1538, 1979.

[52] T. J. Vick, "Documentation for generic hypersonic vehicle model," Air Force Res. Lab., Wright-Patterson AFB, OH, USA, Tech. Rep., 2011.

[53] D. P. Wiese, "Systematic adaptive control design using sequential loop closure," Ph.D. dissertation, Dept. Mech. Eng., MIT, Cambridge, MA, USA, 2016.

[54] J.-J. E. Slotine and W. Li, *Applied Nonlinear Control*. Hoboken, NJ, USA: Prentice-Hall, 1991.

**JOSEPH E. GAUDIO** (Member, IEEE) received the Ph.D. degree in mechanical engineering from MIT, in 2020. He is currently an Engineer at The Boeing Company. His research interests include adaptive systems, optimization, and machine learning.

**ANURADHA M. ANNASWAMY** (Life Fellow, IEEE) is currently the Founder and the Director of the Active-Adaptive Control Laboratory (AACL), Department of Mechanical Engineering, Massachusetts Institute of Technology (MIT), Cambridge, MA, USA. She is the author of a graduate textbook on adaptive control, the co-editor of two vision documents on smart grids and the impact of control technology report, and the coauthor of the National Academy of Sciences Committee report on the Future of Electric Power in the United States, in 2021. Her research interests include adaptive control theory and its applications to aerospace, automotive, propulsion, and energy systems. She has received best paper awards (Axelby; CSM), a Distinguished Member, and the Distinguished Lecturer Awards from the IEEE Control Systems Society (CSS) and a Presidential Young Investigator Award from NSF. She is a fellow of IFAC. She served as the President for CSS, in 2020.

**MICHAEL A. BOLENDER** received the Ph.D. degree in aerospace engineering from the University of Cincinnati, in 2000. He is currently a Senior Aerospace Engineer and the Technical Area Lead for Flight Control in the Aerospace Systems Directorate with the U.S. Air Force Research Laboratory. He is the author or coauthor of over 80 conference papers and journal articles, two book chapters, and two technical reports. His current research interests include the development and application of advanced control for aerospace vehicles, adaptive control, flight dynamics, and modeling and simulation. He is an Associate Fellow of the American Institute of Aeronautics and Astronautics (AIAA).

**EUGENE LAVRETSKY** (Fellow, IEEE) is currently a Boeing Principal Senior Technical Fellow within the Boeing Research & Technology, Huntington Beach, CA, USA. During his professional career at Boeing, he has developed flight control methods, system identification tools, and flight simulation technologies for aircraft and unmanned aerial platforms. He has written over 100 technical articles, a textbook and taught graduate control courses with California Long Beach State University, Claremont Graduate University, California Institute of Technology, University of Missouri Science and Technology, and the University of Southern California. His research interests include robust and adaptive control, system identification, and flight dynamics. He is a fellow of AIAA, in 2018. He was a recipient of the AIAA Mechanics and Control of Flight Award, in 2009, the IEEE Control System Magazine Outstanding Paper Award, in 2011, the AACC Control Engineering Practice Award, in 2012, and the IEEE Control Systems Society Award for Technical Excellence in Aerospace Control, in 2021.